FRYDENDAHL, Odd Jørgen

Influence of the substrate reflectivity on the properties of optically pumped GaAs/GaAsSb nanowire lasers

DEVELOPING A WORKING NANOWIRE (NW)
ARRAY
LASER DEVICE

NTNU
Kunnskap for en bedre verden

FRYDENDAHL, Odd Jørgen

Influence of the substrate reflectivity on the properties of optically pumped GaAs/GaAsSb nanowire lasers

DEVELOPING A WORKING NANOWIRE (NW) ARRAY LASER DEVICE

NTNU

Kunnskap for en bedre verden

Abstract

The present thesis focuses on the influence of substrate on the lasing characteristics of GaAs-GaSb nanowires. The nanowire's lasing potential originates from the six super-lattices inside its structure, each superlattice consisting of ten closely packed GaAsSb layers, working as overlapping quantum-wells. The nanowires were grown using position-controlled self-catalyzed molecular beam epitaxy on a Si substrate. For the experiments presented in this thesis, nanowires were broken off the as-grown substrate mechanically and dispersed onto different substrates as follows. A total of six different samples were studied. Both silicon and a GaAs-AlGaAs distributed Bragg reflector were used as substrates, either pure, or with a 200 nm or 400 nm mask of silica. Analysis was made with photoluminescence spectroscopy at low temperature 20-50 K, using pulsed-laser excitation.

Preface

I, Odd Jørgen Frydendahl, hereby declare that the writing of this master's thesis and its corresponding research work has been performed independently and in accordance with the regulations at the Norwegian University of Science and Technology, NTNU.

This report has been developed from October 2018 to April 2019 at the Department of Electronic Systems, NTNU, under the supervision of Professor Helge Weman and Postdoc Lyubomir Ahtapodov. I would like to extend my deepest gratitude for the outstanding theoretical and practical help my supervisors have granted me during this master thesis.

Furthermore, I would like to thank Postdoc Dingding Ren for helping with the growth process of the nanowires.

<div align="center">

Trondheim, 8th of April 2019

Odd Jørgen Frydendahl

</div>

Contents

List of Tables

List of Figures

Abbreviations

DBR	=	Distributed Bragg reflector
FWHM	=	Full width at half maximum
HWP	=	Half-wave plate
MBE	=	Molecular-beam epitaxy
NIR	=	Near-infrared
NW	=	Nanowire
Q	=	Lasing-quality factor
TE	=	Transverse electric
TM	=	Transverse magnetic
WZ	=	Wurtzite
ZB	=	Zinc Blende

1   Introduction

Semiconductor nanowires (NW) are growing to be a very interesting topic lately, as more and more promising results of lasing are achieved at longer wavelengths (1). As nanoscale emitters of coherent light, NWs have a variety of applications - from bio-medical science to information technology. However, despite being able to achieve lasing at longer wavelengths, it is still challenging to reach near-infrared wavelengths at room temperature. For applications such as optical interconnects in future compact nanophotonic circuits and on-chip communication systems, and for bio-medical applications, it is necessary to develop suitable laser sources in the NIR spectrum.

So far, a variety of different NW laser structures have been demonstrated, such as ZnO and ZnS lasers for ultraviolet spectra, or GaAs and GaSb for near-infrared spectra. The difficulty, however, is to achieve a low lasing threshold with high lasing-quality (Q) factor and wide wavelength tunability.

The focus of the work reported in this thesis is on optimizing lasing for GaAs-GaAsSb lasers by studying the effect of the substrate on the nanowire lasing parameters. Analysis of single nanowires lying on two different types of substrates, Si and a GaAs/AlAs DBR optimised for 950 nm, with a silica spacer of variable thickness from 0 to 400 nm, at 20-50 K. The results are shown for each individual nanowire, and for NWs that achieved lasing, the lasing peak are integrated and plotted as a function of the excitation power. The Q-factor is also evaluated, together with the FWHM.

2 Theory

2.1 Distributed Bragg reflector

The substrate is of particular importance as it is one the deciding factors for whether or not the optical energy can be confined inside the nanowire. First off: if we consider a nanowire lying on the substrate, a reflective substrate will prevent the guided waves inside the nanowire from leaking out. Additionally, it will help the light emitted by the nanowire to reflect outwards from the substrate, increasing the measured signal emitted from the nanowire itself. Secondly, if we now consider a nanowire standing perpendicular to the surface, a reflecting substrate will help creating a mirror at the end of the wire. This is one of the main prerequisites for lasing, and it is therefore a very helpful feature.

A Distributed Bragg reflector (DBR) is a structure used in the application of selectively reflecting wavelengths within a certain range of interest while letting others pass. The DBR is a one-dimensional photonic crystal, built up layer by layer consisting of different materials such that the refractive index varies periodically in one direction. The reflected wavelength can be controlled by certain factors, such as: different indices of refraction and their thicknesses. Each boundary between two layers partly reflects and partly transmits light incident at it, and by varying the refractive index, thickness and number of layer pairs, it can be arranged that wavelengths in a certain range are nearly totally reflected by the DBR.

It is known that the Bragg reflector will have widest reflection band given the two selected materials under the condition where the optical thickness is approximately a quarter of the wavelength (2). This means that the the optimum thickness for each layer can be set:

$$d = \frac{\lambda}{4 \cdot n} \tag{1}$$

where d is the thickness of the layer, λ is the vacuum wavelength of the incident light, and n is the refraction coefficient. Due to this proportionality, reflected waves at the selected

wavelength of interest will interfere constructively, yielding the highest reflectance.

2.2   Omnidirectional Reflector

Further we need to ensure that our reflector works for every angle of incident light, as well as for both transverse electric (TE) and transverse magnetic (TM) polarization. If we consider the case where we have a nanowire lying on the substrate, the angle at which the light impinging on the boundary between the nanowire and the substrate can differ considerably from $0°$. If this is not taken into consideration when choosing materials for the reflector, the nanowire emission may end up outside the reflection band of the DBR which depends on the angle of incidence.

To understand the physics behind this, we need to look into photonic band gaps, and how they work. Photonic band gaps are very similar to electronic band gaps, and operate very much in the same way. As the electronic band gap represent the forbidden states of electron energy, the photonic band gap represents forbidden modes in the optical medium where no waves of that particular wavevector can propagate. The forbidden regime is a direct consequence of the spatial periodicity of the refractive index and builds up as a result of the energy distribution for high and low frequencies around high and low values of the electric permittivity.

If we consider the photonic modes that exists directly below and above the band gap, where $k = \pi/a$, the waves will
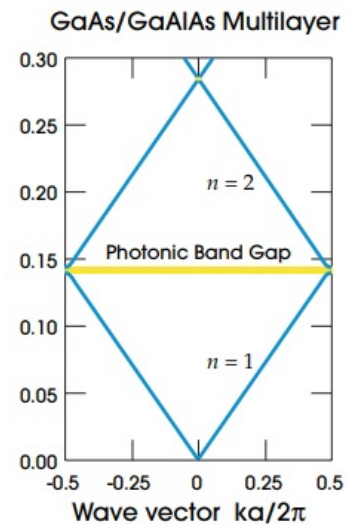
Figure 1: Photonic band gap in a multilayer GaAs and GaAlAs structure. The x-axis is limited by the first Brillouin zone. The yellow line is the photonic bandgap, while the two different refractive indexes being n=1 and n=2.

have a length that is twice the crystal's lattice constant a. The domain of $k = [-\pi/a, \pi/a]$ is defined as the first Brillouin zone (4), and higher values of k will only lead to a repetition of identical Bloch modes. Here we also assume that the reflection is on-axis, meaning that incidence is perpendicular to the surface.

The only two ways of centering a mode in the given system without breaking the symmetry would be for the nodes to lie in each layer where ε is low (Fig: 2a), or where ε is high (Fig: 2b). Since modes with low frequency concentrate their energy in the regions where ε is high (3), and modes with high frequency concentrate their energy in the regions where ε is low, a jump in frequency will be created in the boundary between the two materials with different values of the dielectric permittivity. This creates the photonic band gap, and frequencies within this gap will attenuate exponentially inside the structure.

(a) *E*-field for mode at top of band 1
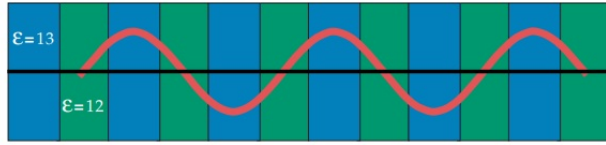
(b) *E*-field for mode at bottom of band 2
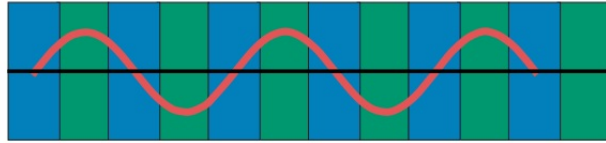
Figure 2: Electronic fields for modes at top of band 1 and bottom of band 2 as seen in figure 1.

The band gap is often characterized by the gap-midgap ratio:

$$\frac{\Delta\omega}{\omega_m} \approx \frac{\Delta\varepsilon}{\varepsilon}\frac{\sin(\pi d/a)}{\pi}, \tag{2}$$

where $\Delta\omega$ is the width of the band gap, and ω_m is the frequency at the middle of the gap. The experession $\frac{\Delta\varepsilon}{\varepsilon}$ comes from the contrast between the dielectric permittivity of the two materials. Equation 2 is only valid if the contrast between the materials is weak, meaning that either $\Delta\varepsilon/\varepsilon << 1$ or the thickness d/a is small. The gap-midgap ratio is

often the best reference to the "size" of the band gap. The reason for this is that if we were to look at the gap itself, $\Delta\omega$, the frequency would scale as the crystal expanded by a factor s, leading to a width of $\Delta\omega/s$. If the system is scaled, the frequencies are scaled accordingly, but the gap-midgap ratio remains the same.

So far we have only looked into cases where the incident light is perpendicular to the layers of the structure, $\hat{\mathbf{z}}$. Letting $\mathbf{k} = k_y\hat{\mathbf{y}}$ we end up with band gaps looking like the right side of figure 3. Here the blue line represents all the x-polarized modes (transverse magnetic modes), and the red line represent all the y-polarized modes (transverse electric modes). The bending form of the bands is also a result of the angle of incidence. As we can see, the angle of incidence alters the allowed modes, resulting in a different photonic gap.
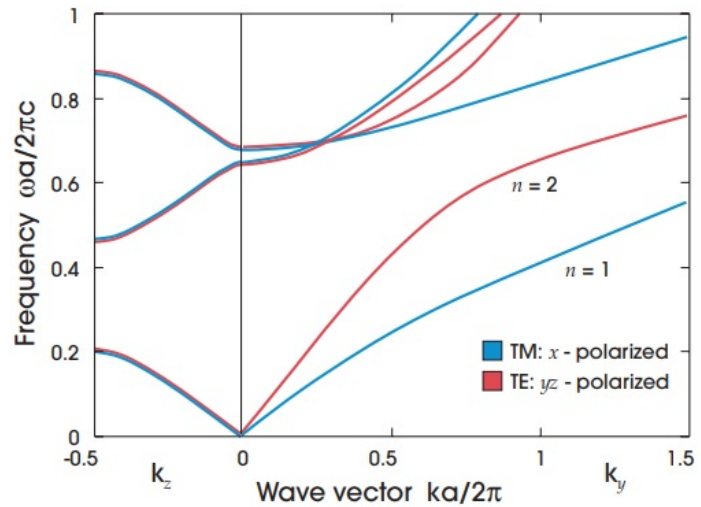
Figure 3: The band structure of a multilayered film. For the on-axis bands $(0,0,k_z)$ on the left side, the bands are overlapping each other. As soon as we account for modes that is not parallel to the direction of propagation, the band gaps start to split into two distinct polarizations. The blue line being the TM-polarized band, while the red line is the TE-polarized gap.

An important difference between on-axis and off-axis propagation is that there exists no band gaps for off-axis propagation when all possible k_y-values are included. The reason behind this is that for off-axis directions the spatial periodicity of the dielectric constant is broken and the structure cannot coherently scatter the light and split open a gap. Despite this, it is still possible to create a multilayered film that reflects external plane waves that are incident from any angle. These structures are called omnidirectional multilayer mirrors.

For omnidirectional multilayer mirrors to work, there are two main criterias that must be fulfilled in order to achieve perfect reflection. First, modes with wavevector parallel to the layers must be conserved at any interfaces parallel to the layers. Thus the light source needs to be far enough away so it is not interfering with the translation symmetry of the structure. Second, light that is incident from air must have angular frequency $\omega > c \mid k_{\parallel} \mid$ corresponding to the freely propagating modes above the light line (marked as the red line in figure 4). All the modes beneath the light line are evanescent, which means they are bound to an interface and decay exponentially away from it. To make sure that we have photonic bandgap for freely propagating modes above the light line, it is of particular importance that the dielectric contrast between the two materials used must be sufficiently large. Looking at figure 4, the dielectric contrast must be large enough so that the point marked L (the lowest point at which the light line crosses path with the allowed band), is below the point marked U (the lowest point of the allowed band). It is also important that the smallest dielectric constant of the two materials is larger than the dielectric constant of the ambient medium by a critical amount. If these conditions are fulfilled, adding up enough layers in the omnidirectional multilayer mirror will result in a perfectly reflecting substrate.
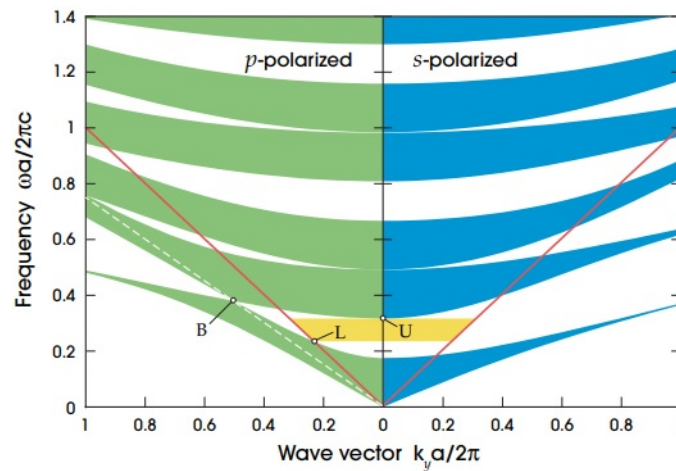
Figure 4: Band-diagram for off-axis propagation vectors $(0, k_y, k_z)$ in a quarter-wave stack. The blue side represent the transverse magnetic modes, while the green side represent the transverse electric modes. The yellow zone represent the first frequency range of omnidirectional reflection. The light line is marked as red. (2)

2.3 The Nanowire

2.3.1 Growth and Structure

The growth of nanowires was done using a self-catalysed molecular-beam epitaxy (MBE) technique. The technique is still considered relatively new, and is an alternative to Au-catalysed MBE growth.
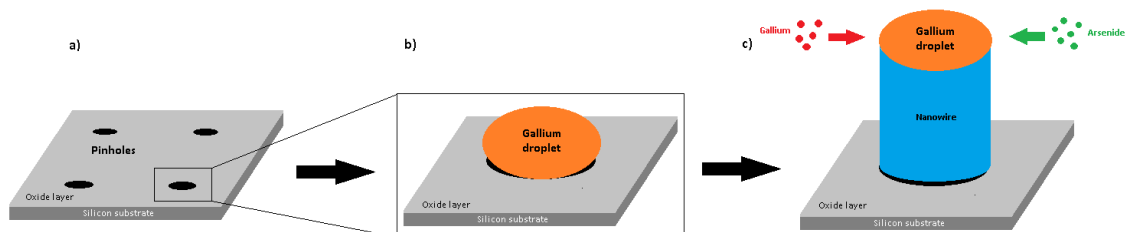
Figure 5: Schematic of the self-catalysed molecular-beam epistaxy based of gallium. a) natural or deposited oxide layer with pinholes laying on a silicon substrate, b) build up of gallium droplets inside the pinholes, c) nanowires grown bottom-up after supersaturation.

To start off, an oxide mask is deposited onto the Si substrate. A pinhole array is then fabricated in the oxide mask by using electron beam lithography (fig. 5a). It is important to make sure that the pinholes have sufficiently large spacing between them. This way the nanowires will grow separately away from each other, reducing the nanowire-to-nanowire variability of optical and structural properties due to, among others, droplet size variation, competition between closely spaced nanowires and

Ga^{3+} As^{3-}
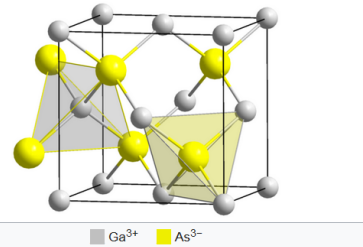
Figure 6: Zincblende crystal structure. The name comes from a ZnS composition where the crystal structure is based on a fcc lattice.

shadowing by neighbouring nanowires. After the pinholes are made, Ga is deposited on top of the oxide layer with pinholes, and the heat is turned up to around 620 °C. The gallium will then start to migrate towards the pinholes, forming a droplet inside each hole (fig. 5b). The molecular beams of the precursor materials are then switched on, and will shortly after enter the droplets (fig. 5c). The droplet will reach supersaturation, and from this point a GaAs (or GaAsSb) will grow perpendicular to the surface at the vapour-liquid-solid boundary. The fabricated GaAs nanowire got a zinc blende crystal structure (ZB, fig. 6), and grow in the <111>B crystallographic direction.

During the growth process a different material will be inserted into the wire, creating an axial insert. If sufficiently short, axial inserts can act as quantum wells. Multiple quantum wells close enough to each other so that the electronic states of neighbouring wells interact are called electronic superlattices.

At the end of the process the temperature is lowered so the Ga droplet solidifies. The axial nanowire growth will then cease, making it possible to deposit uniform shell on the sides of the nanowire. GaAs does not have any native oxides at its surface, resulting in band gap defects near the surface. These defects increases the path for non-emitting recombinations (recombination of electron-hole pairs are discussed further in section 2.4.2

- 2.4.6), making the life time of excited particles shorter, which in turn weaken the signal. To prevent this from happening, a material with a large band gap that causes as little strain as possible on the NW should cover the surface of the NW. The best material for this purpose is AlGaAs, hence growing a radial AlGaAs shell is the most common way of passivating the surface of GaAs nanowires.

Figure 7: Simplistic view of how an axial-inserted heterostructure looks like. (9)

The secondary material used to create the superlattice is GaAsSb, and it is introduced for short period of time during the GaAs nanowire growth at constant temperature. At the end of this process the growth is interrupted for a short period of time to ensure a more abrupt change in the composition between the two materials in the nanowire. Without interrupting the process, there will be an increased chance of having the so-called reservoir effect which causes a gradual compositional variation instead of an abrupt sawtooth profile.
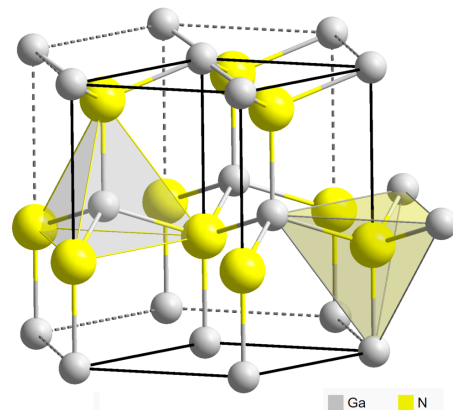
Figure 8: Wurtzite is an other crystal structure much like Zinc Blende, but is based on hcp array rather than a fcc structure.

Despite the fact that the growth conditions are tuned to yield nanowires of zinc blende crystal structure, there are often defects in the form of wurtzite inclusions of sizes varying from a single crystallographic period (i.e. a twin plane) to segments with high density of

twin planes commonly referred to as mixed zinc blende/wurtzite regions and extended wurtzite segments. (fig: 8). The stacking sequence of WZ can be described as ABABAB, where A and B are two differently arranged bilayers containing both Ga and As atoms. ZB however, is described as ABCABCABC where an additional monolayer C is present. The faults following WZ then often looks like ABAB<u>ACB</u>AB, or any other combination which introduce a random C into the WZ structure.

Wurtzite structure is often more common at the ends of the nanowire. These defects are often much longer than the single combinations described above, and got the characterization of ABAC repeated in chains. Their occurrence varies significantly from nanowire to nanowire, due to local variations in the growth conditions.

For the work done in this thesis, wurtzite crystal structure is present in all the GaAs layers of the nanowires. The defect crystal structure will not affect the result due to having a laser as the power source for the optical pumping of the nanowire. For electrically driven nanowire-based optoelectronic devices, the wurtzite structure would add resistance due to its different band gap compared to zinc blende crystal structure. Additionally, the nanowires in this thesis has an active medium made of GaAsSb, which has a very stable zinc blende crystal structure when grown. The superlattices will therefore be nearly defect-free.
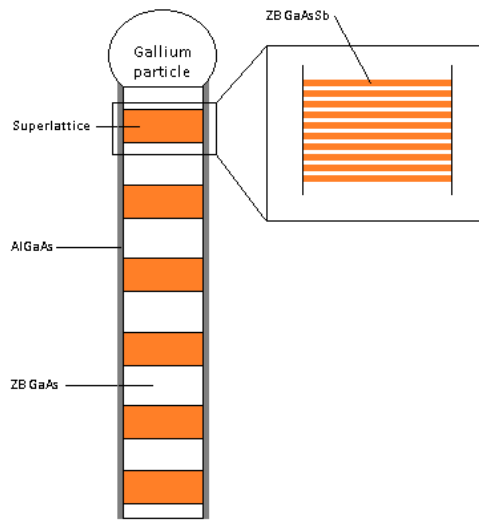
Figure 9: Schematics of a grown nanowire studied in this thesis. Each nanowire contain 6 super-lattices, each made up of 10 GaAsSb layers. The nanowire also got an AlGaAs coating to prevent the bad surface conditions of GaAs.

2.4 Optical Properties of Semiconductor Nanowires

2.4.1 Electronic Band Gaps

To understand the mechanisms behind the relevant optical processes such as light emission and absorption, discussed in this thesis, we first need to dive into the electronic properties of the chosen materials. GaAs and GaAsSb are both semiconductors with crystalline structure, meaning that all atoms are arranged in a strict periodic three-dimensional lattice. The atoms in the lattice are located relatively close to each other, meaning that the outer electron shell for each atom is overlapping with those of its closest neighbours. This results in the unique property of semiconductors, where the electron energy forms allowed and forbidden quasi-continuous electronic bands.

The electronic band gaps can be understood more in detail by looking into the solution of the time-independent Schrödinger equation for all electrons and all nuclei in the semiconductor material. The Hamiltonian for all electrons and nuclei, which is an operator

describing the kinetic and potential energies inside a given system, can be written as:

$$H = -\sum_i \frac{\hbar^2}{2m_i}\nabla_i^2 - \sum_I \frac{\hbar^2}{2M_I}\nabla_I^2 + \sum_{i<j} \frac{e^2}{4\pi\varepsilon_0|\vec{r}_i - \vec{r}_j|} - \sum_{I,i} \frac{Z_I e^2}{4\pi\varepsilon_0|\vec{R}_I - \vec{r}_i|} + \sum_{I<J} \frac{Z_I Z_J e^2}{4\pi\varepsilon_0|\vec{R}_I - \vec{R}_J|} \quad (3)$$

where i and j refer to the electrons, I and J refer to the atomic nuclei, m and M are the electron and nuclear mass respectively, $\vec{r}$ and $\vec{R}$ are the electron and nuclear radius-vectors respectively, and Z is the atomic number.

The first two terms on the right-hand side correspond to the kinetic energy operators of the electrons and the nuclei, respectively. The last three terms on the right-hand side describes the electrostatic Coulomb forces between electrons in the third term, electrons and nuclei in the fourth term, and between the nuclei in the last term.

Since this Hamiltonian is too complex and contains too many variables if we were to bring all atoms into consideration for a single piece of material, approximations are needed in order to solve the problem. The Kronig-Penney model is a simple way to describe such a problem. The model focuses on a single electron inside a one-dimensional periodic potential well, shaped like squares that represent the atoms of the crystal lattice. The result of calculating the electron dispersion from the Kronig-Penney model can be seen in figure 10, together with the dispersion of a free electron.
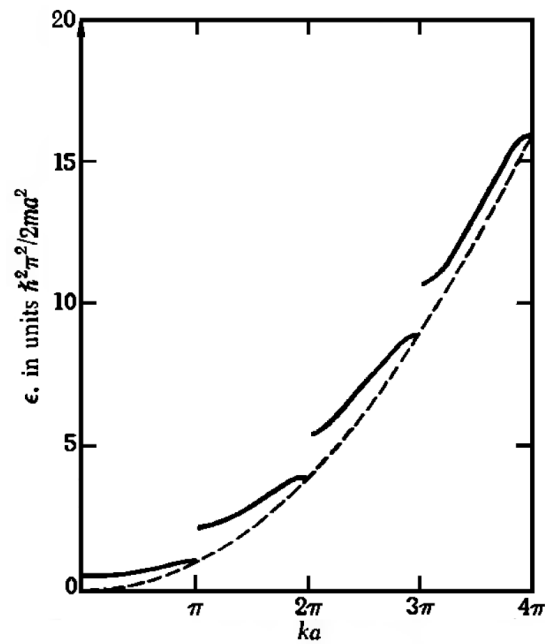
Figure 10: Solid line represent electron dispersion calculated from the Kronig-Penney model, while the dashed line represent free electron dispersion. (7)

Because the periodic potential modulates the electron dispersion inside the one-dimensional chain of atoms, the Kronig-Penney dispersion ends up being a multiple-valued function, periodic in the k-space. The unit cell of the k-space is the Brillouin zone introduced in 2.2, and it is enough to consider only the Brillouin zone in order to understand the electronic properties of the material, due to the periodicity of the lattice. Focusing on the Brillouin zone narrows down the consideration to $k = \pm\frac{\pi}{a}$, where a is the lattice constant. Gaps of forbidden energy form at these points, seperating the branches of the dispersion curve above and below. Figure 11 show the three-dimensional band structure of GaAs. The branches of the dispersion curve are replaced with quasi-continuous bands of allowed energy values.
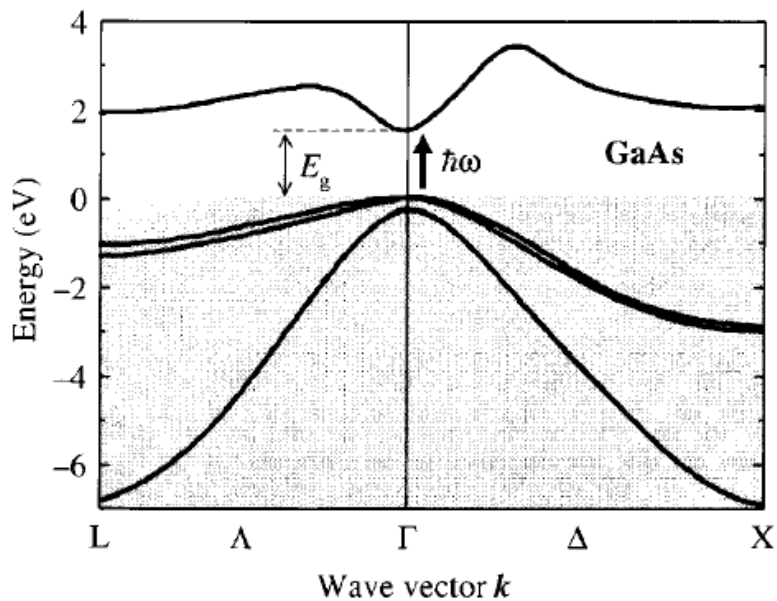
Figure 11: Electronic band gap structure of GaAs. (8)

For semiconductors, these bands are either completely filled for the valence band, or completely empty for the conduction band at $T = 0K$. Additionally, a forbidden gap exist between the highest fully occupied and the lowest completely vacant bands. Thus, the highest fully occupied and the lowest completely empty bands at T = 0 K are called valence and conduction band, respectively, and the forbidden band separating them is called the band gap. If the smallest existing band gap is centered in the Brillouin zone, the gap is said to be direct (fig. 12a). However, if the smallest gap lies outside the center of the Brillouin zone, the gap ends up being indirect as figure 12b shows. An electron excited in an indirect bang gap needs the energy of a phonon in order to preserve the momentum. A phonon is the excitation quantum of the crystal lattice vibrations, in the same way as a photon is the excitation quantum of electromagnetic radiation.

The band gaps of interest for this thesis are:

Material:	Room temp.	$T = 0K$.
ZB GaAs	1.425eV	1.519eV
GaSb	0.725eV	0.813 eV

14
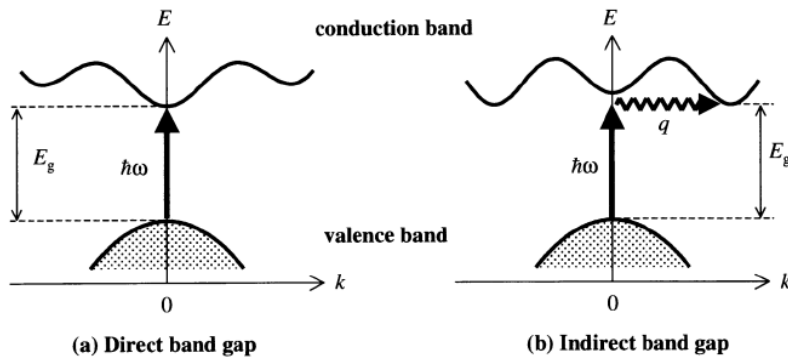
Figure 12: a) Shows a direct band gap in a typical semiconductor, while b) show an indirect band gap. When an electron gets excited with enough energy to make a "jump" up to the conduction band, it can recombine with its former position right away for the direct band gap. As for an indirect band gap, the electron needs to release energy in form of a phonon in order to recombine. (8)

2.4.2 Heterojunctions

When two materials of different electronic band gaps are adjacent to each other, such as GaAs and GaAsSb are in the nanowire, they make up a heterojunction in the band-diagram. This heterojunction consist of bands with different width, forming either one of the two possible alignment diagrams shown in figure 13. For the first type of heterojunction, one of the materials has in general much smaller band width than the other. It is also important to notice that the conduction band level of the narrower band gap material lies lower than the wider one, and at the other side the valence band lies higher up. However, for the second type of heterojunction, one band gap can both have a lower conduction band and lower valence band.

The efficiency of optical transitions between the two materials are heavily dependent of what type of heterojunction that is present. For Type-I, both the electrons and the holes are able to diffuse into the lower band gap material, letting the electron-hole pairs be roughly at the same position within the junction. As for Type-II, the electron-hole pairs will be separated, meaning higher recombination time and lower probability of recombination. In our case, the amount of antimony is the deciding factor of which type of heterojunction the nanowire has. If the amount of Sb exceeds 34%, the heterojunction between ZB

GaAs and GaAsSb shift into Type-II with the conduction band of GaAsSb lies higher. This means that only the holes will be able to diffuse from the GaAs and into GaAaSb, not the electrons.
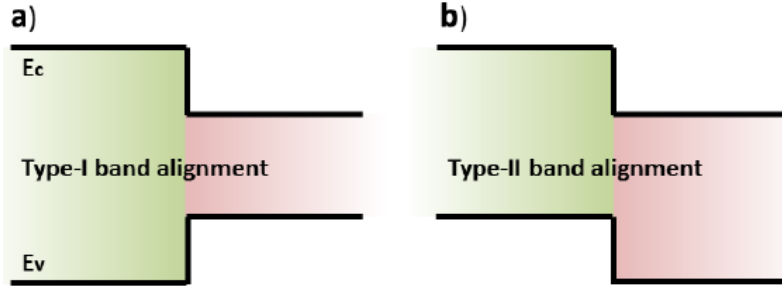
Figure 13: Two possibilities of heterojunction between two materials of different band gap width. a) Type-I and b) Type-II(9)

2.4.3 The Effective Mass

As seen in section 2.4.1, the electron dispersion in crystalline solids differs from the free-electron model. When an electron travels in a periodic potential over distances longer than the lattice spacing a, it is necessary to introduce the effective mass in order to simplify the band structure. The electron dispersion close to the maximum or minimum of a band gap occurring at $\vec{k} = \vec{k}_0$ can be expanded in a Taylor series as follows:

$$E(\vec{k}) \approx E(\vec{k}_0) + \frac{1}{2} \sum_{i,j} \frac{\delta^2 E}{\delta k_i \delta k_j} (k_i - k_{0,i})(k_j - k_{0,j}), \tag{4}$$

where $E(\vec{k})$ is usually set as the zero-energy reference point, and falls off. This gives $E = \frac{\hbar^2}{2m} (\vec{k} - \vec{k}_0)^2$, if we define the inverse effective mass as:

$$(m_{ij}^{-1}) = \frac{1}{\hbar^2} \frac{\delta^2 E}{\delta k_i \delta k_j} |_{k=k_0} \tag{5}$$

Keep in mind that this approximation of electron mass is only valid for carries close to the band maximum and band minimum. Luckily, most of the optical processes in this thesis occur after thermal relaxation, meaning that the electrons falls within the application area

of the effective mass.

2.4.4 The Optical Joint Density of States

One of the main criteria of calculating the density of states for a finite volume of a semiconductor material is the materials boundary conditions. A cube with volume L^3, where L is one of the sides of the cube, will result in the quasi-wave vector k taking a finite set of values spaced $\Delta k = \frac{2\pi}{L}$ apart. In reciprocal space this gives $(\frac{2\pi}{L})^3$ as volume per state. If we look at a sphere with volume $\frac{4}{3}\pi k^3$ in k-space, it will contain $N = g_s \frac{4}{3}\pi k^3 (\frac{2\pi}{L})^{-3}$ states. g_s is the spin degeneracy of energy states. The density of states is defined as the number of states per unit wave number per unit volume in real space, which gives $\frac{dN}{dk} = g_s \frac{4\pi k^2}{(2\pi)^3}$. From (4), it follows:

$$D(k) = g_s \frac{4\pi k^2}{(2\pi)^3}, \text{ 3D (bulk)}$$

$$D(k) = g_s \frac{2\pi k}{(2\pi)^2}, \text{ 2D (quantum wells)} \tag{6}$$

$$D(k) = g_s \frac{2}{2\pi}, \text{ 1D (quantum wires)}$$

The density of states can also be given in terms of energy instead of the wave number:

$$D(E) = g_s \frac{1}{(2\pi)^2} \left(\frac{2m^*}{\hbar^2}\right)^{3/2} \sqrt{E}, \text{ 3D (bulk)}$$

$$D(E) = g_s \frac{1}{4\pi} \left(\frac{2m^*}{\hbar^2}\right), \text{ 2D (quantum wells)} \tag{7}$$

$$D(E) = g_s \frac{1}{2\pi} \left(\frac{2m^*}{\hbar^2}\right)^{1/2} \frac{1}{\sqrt{E}}, \text{ 1D (quantum wires)}$$

Figure 14 is sketched based on equation (7), and makes it evident that the 3D bulk density of states differs a lot from the lower-dimensional materials. What this means is that at the edges of the lower-dimensional materials a much greater number of states are available for the carries. This results in higher probability for radiative recombination, which, in turn, highlights the benefits of utilizing quantum dots, wires and wells in light emitting optoelectronic devices.
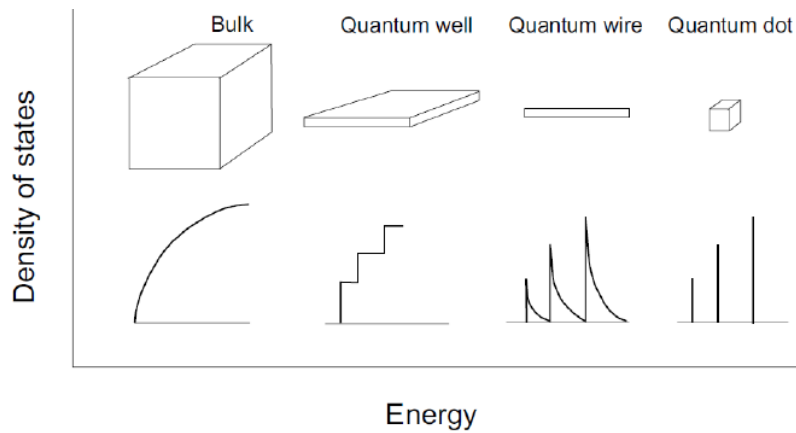
Figure 14: Density of states as function of energy. (10)

2.4.5 Carrier Statistics and the Fermi Level

The energy distribution of particles and quasi-particles is given by either of the three expressions: Bose-Einstein distribution, Fermi-Dirac distribution or Maxwell-Boltzmann distribution. The Bose-Einstein distribution describes the behaviour of particles and quasi-particles such as photons, phonons and excitons. The Fermi-Dirac distribution describes the behaviour of particles and quasi-particles such as electrons, holes, protons and neutrons, while the Maxwell-Boltzmann distribution describes the behaviour of classical, distinguishable particles.

For the purpose of this thesis, we will look more into the Fermi-Dirac distribution given by:

$$f_{FD} = \frac{1}{exp(\frac{E-F}{kT})+1}. \tag{8}$$

As mentioned above, this equation describes the energy distribution of fermions such as electrons, holes, protons and neutrons. Fermions are subject to Pauli's exclusion principle, stating that two particles of same set of quantum numbers cannot coexist inside a material. This means that electrons will fill up the the energy bands from bottom to top, where no more than two electrons can have the same energy level. This is due to the fact that the electron energy is spin-degenerate, whereby electrons have half-integer spin with

two possible orientations, e.g. "up" or "down". Another property worth mentioning is that the Fermi energy, F, always have the probability of occupation equals to 0.5, independent of temperature. The Fermi energy is also dependent on the carrier concentration, so if impurities such as dopants are introduced to the material, the Fermi level will shifts either up or down.

2.4.6 Fermi's Golden Rule

Now that we have looked into the density of states and the energy distribution, we can start to understand the model of optical absorption and emission. Fermi's Golden Rule is a way of describing optical absorption and luminescence for a semiconductor medium, and is given by (11):

Optical absorption:

$$W_{v \to c} = \frac{2\pi e^2}{\hbar^2} |z_{cv}|^2 |E_z|^2 D(\omega - \omega_g) f_{FD}(E_v)[1 - f_{FD}(E_c)] \tag{9a}$$

Optical emission:

$$W_{c \to v} = \frac{2\pi e^2}{\hbar^2} |z_{cv}|^2 |E_z|^2 D(\omega - \omega_g) f_{FD}[1 - f_{FD}(E_v) f_{FD}(E_c)] \tag{9b}$$

Starting off with the variables we discussed above, $D(\omega - \omega_g)$ is the optical joint density of states, where ω is the emission or absorption frequency. ω_g is the frequency that corresponds to the band gap of the material.

The Fermi-Dirac functions is given by two variables, one for the conduction band and one for the valence band. The product of these two functions gives the probability that there will be an electron occupying the initial state in the valence band, and that it has an empty state in the conduction band to get excited in to. In the case of light emission,

the product of the functions describes the probability of having an electron in a high energy state in the conduction band while there is an empty state down in the valence band.

$|z_{cv}|^2$ is the oscillator strength, a quantum-mechanical matrix element of the operator that describes the potential of the light-matter interaction. It contains the selection rules of both absorption and emission of light by semiconductors. The resonant absorption and emission of light between energy bands are forbidden if the matrix element for the transition between those two bands vanishes.

$|E_z|^2$ is the electric field amplitude. The variable vary with the type of radiation that interacts with the matter. It's the electric field of the blackbody radiation that the material is subjected to for spontaneous emission, and the field generated due to and external light wave incident on the material for absorption and stimulated emission.

For an electron in an occupied state of the valence band to be able to absorb the energy of an incoming light wave, there must be a free state in the conduction band where the electron can be excited in to. Since there will be a wide range of occupied states in valence band and free states in the conduction band, there will also exist a wide range of different transition routes that correspond to different wave frequencies, starting at the wavelength matching the band gap. Thermal relaxation occurs at a shorter period of time compared to how fast light would be emitted, meaning that the recombination will happen between electrons at the bottom of the conduction band, and holes at the top of the valence band. For a direct band gap, the recombination occurs directly between the electron and the hole. While in an indirect band gap, the electron needs to change momentum with the help of a phonon in order to recombine with the corresponding hole. Since another particle is in need to make a recombination of an indirect band gap occur, the probability of this happening also decreases. This is why direct band gaps are better for light emitting devices.

2.5 Stimulated emission

2.5.1 The Active Medium

One of the main criteria for a laser device to achieve lasing is to make sure that the radiant flux inside the lasers medium is increasing. In normal circumstances, when the light passes through a medium, the radiant flux decreases due to absorption in the medium and scattering of the light. Looking at the smaller scale, the change of radiant flux, $d\Phi$, is proportional to the radiant flux, Φ impinging on the same thin layer of the medium, dx:

$$d\Phi(x) = -\alpha(x)\Phi(x)dx. \tag{10}$$

The constant α is the absorption coefficient, and for most cases where the radiant flux decreases upon transmission through the material, it is a positive quantity. If we assume that the medium is homogeneous, meaning that there is no change in α throughout the medium, we can integrate (10) to get Beer's law:

$$\Phi(x) = \Phi(0)exp(-\alpha x). \tag{11}$$

As we can see from equation (11), if the absorption constant α was to be negative, the radiant flux would increase as the light propagates through the medium. α is then called gain coefficient, and the medium is said to be an active medium. How to achieve this is discussed in the next section.

2.5.2 Stimulated Emission

Radiative transition from a higher energy level E_i to a lower energy level E_j of a system of identical atoms is either a spontaneous transition that occurs without any external driving mechanism, or a stimulated transition, i.e. driven by an external field. For a stimulated transition, the rate of stimulation is proportional to the spectral energy density $\rho(\nu)$ at the resonant frequency $\nu_{ij} = (E_i - E_j)/\hbar$ present inside the material. Under thermal equilibrium, the number of emitted light quanta per unit time equals the number of absorbed

light quanta per unit time. They are also proportional to the external spectral energy density $\rho(v)$. The equilibrium condition in the presence of stimulated transitions can be expressed as follows:

$$A_{ij}n_i + B_{ij}\rho(v_{ij})n_i = B_{ji}\rho(v_{ij})n_j. \tag{12}$$

A_{ij}, B_{ij} and B_{ji} are the Einstein A- and B-coefficients, n_i and n_j denote the number of atoms with energy E_i and E_j, respectively. The left-hand side term represents the emitted photons, while the right-handed side represent absorbed photons.

To be able to solve equation (12), we assume that the atoms in the system are distributed according to the Maxwell-Boltzmann distribution given by:

$$f_{MB} = A exp(-\frac{E}{kT}), \tag{13}$$

which gives:

$$\rho = \frac{[\frac{A_{ij}}{B_{ij}}]}{[\frac{B_{ji}}{B_{ij}}]\frac{g_j}{g_i}exp(-\frac{E_j-E_i}{kT}) - 1}. \tag{14}$$

g_i and g_j denote the degree of degeneracy of the levels E_i and E_j, respectively. Equation (14) must agree with both Wien's displacement law and Rayleigh-Jeans' law at high temperatures, giving:

$$\frac{A_{ij}}{B_{ij}} = \frac{8\pi h v^3}{c^3}, \tag{15}$$

and

$$B_{ji}g_j = Bijg_i. \tag{16}$$

Given equations (12), (14), (15) and (16), we get:

$$n_{abs}(v_{ij}) = B_{ji}\rho(v_{ij})n_j - B_{ij}\rho(v_{ij})n_i = B_{ji}\rho(v_{ij})(n_j - \frac{g_j n_i}{g_i}). \tag{17}$$

Equation (17) describes the number of photons from the incident radiation with spectral density ρ that get absorbed by a unit volume of the system per unit time with account of the stimulated emission. We can see that if $n_i > n_j$, we end up having a gain in the

system. The condition $n_i > n_j$ is called population inversion as it corresponds to higher number of particles in the high energy state E_i, and is one of the key prerequisites for lasing.

2.5.3 Optical Feedback

Another important prerequisite for laser devices to achieve lasing is optical feedback. In the last section we discussed how an active medium helps with amplifying the radiant flux as light wave propagate through the material. In order to maintain the gain in a continuous loop, the optical energy has to be at least to an extent confined inside the active medium, which is usually achieved by placing the active medium in an optical cavity with highly reflective mirrors. Every time a light wave hits a mirror, it acquires a phase shift. It is therefore important to make sure that the light waves traveling inside the active medium have matching phases while they make a roundtrip, such that constructive interference is achieved. The most common way of doing this is by having one near perfect reflecting mirror and one less reflective mirror parallel to each other, facing inwards, such that light waves can travel forth and back inside the active medium. One of the mirrors needs to be less reflective to create an output for the laser beam. This setup is called Fabry-Perot resonator. For a Fabry-Perot resonator of length L, assuming there are no losses, the phase of a single roundtrip is given by:

$$\phi = k2L = \frac{4\pi n \nu L}{c},$$ (18)

where n is the refractive index of the active medium, ν is the frequency of the light waves, and c is the speed of light in vacuum. The phase ϕ needs to be a multiple of 2π in order to maintain the constructive interference of the traveling waves. Because of this condition, there will only be a set of frequencies that are able to gain optical feedback inside the cavity, called modes. In the case of a Fabry-Perot resonator, the modes are equidistant, separated by $\nu_{FP} = c/2nL$.

However, there will always be losses as light propagates inside the cavity due to imperfect mirrors, absorption and/or scattering inside the active medium. From (6) we have have an infinite number of waves with amplitudes that decrease at a geometric rate, $U_1 = \sqrt{I_0}$, $U_2 = hU_1$, $U_3 = hU_2 = h^2U_1$, ..., giving:

$$U = U_1 + U_2 + U_3 + ... = \sqrt{I_0}(1 + h + h^2 + ...) = \frac{\sqrt{I_0}}{1-h}, \tag{19}$$

where $h = |h|exp(j\phi)$. The total intensity is U squared:

$$I = |U|^2 = \frac{I_0}{(1-|h|)^2 + 4|h|\sin^2(\phi/2)}. \tag{20}$$

We can write this equation:

$$I = \frac{I_{max}}{(1 + (2\mathscr{F}/\pi)^2 \sin^2(\phi/2)}, \tag{21}$$

where the quantity

$$\mathscr{F} = \frac{\pi\sqrt{|h|}}{1-h} \tag{22}$$

is the finesse. For sufficiently large finesse, $\mathscr{F} >> 1$, equation 21 leads to:

$$\delta\nu = \frac{\nu_{FP}}{\mathscr{F}}. \tag{23}$$

This equation express the full width at half-maximum (FWHM) of the intensity peaks. We can also define the Q-factor from this:

$$Q = \frac{\nu_0}{\nu_{FP}}\mathscr{F} = \frac{\nu_0}{\delta\nu}. \tag{24}$$

As seen from 24 the lasing quality-factor, Q, is proportional to the finesse. In this report we have chosen to use the Q-factor for the NW analysis.

3 Experimental Methods

Between 40-50 nanowires were analyzed through photoluminescence spectroscopy, where 15 of them were at $T = 20K$, and another 15 at $T = 50K$. Only samples that showed promising results at room temperature were taken through low-temperature analysis. All the samples consisted of single nanowires.

3.1 Laboratory Setup
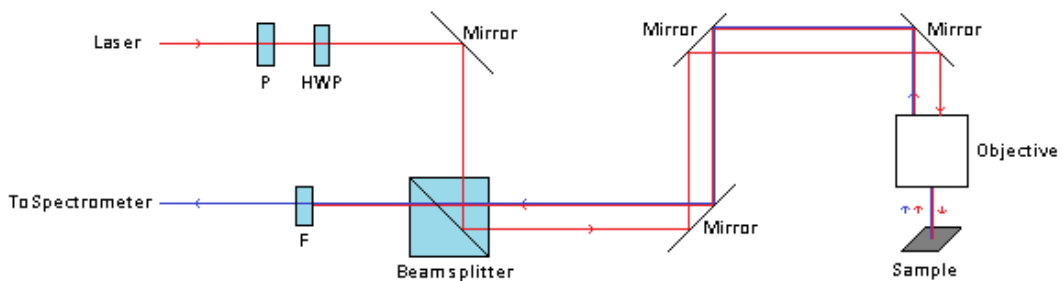
Figure 15: Schematic for the laboratory setup. P = polariser, HWP = Half-wave plate, F = filter for the source-laser/gray-filter. The laser beam is drawn straight down from the objective for simplistic reasons. In reality it is focused down onto the sample. Red lines represent the source-laser, while blue lines represent the light emitted from the nanowire. Keep in mind that the blue color is used only to differentiate between the two beams. The wavelength is usually between 880-940nm, meaning it is in the near-infrared spectrum.

Figure 15 shows the schematic of the laboratory setup used for analyzing the nanowire samples in the thesis. The samples were placed inside an optical cryostat for the purpose of having cold-temperature measurements available, and to be able to position the sample precisely relative to the excitation beam using a piezo controller. The excitation beam was guided through an adjustable gray-filter in order to control the intensity of the excitation beam before it hits the sample. The gray-filter itself does not tolerate high intensity, so a polarizer was installed before the gray-filter as a first stage of intensity reduction. However, since the polarisation orientation is fixed, while a nanowire of interest on the sample surface may be oriented in any direction, it is important to add a half-wave plate after the polarizer, to control the polarization of the light beam. It is of great impor-

tance that the polarization of the light beam is oriented along the nanowire axis in order for the nanowire to absorb as efficiently as possible. The reason for this is the dielectric mismatch effect, arising due to the small dimensions and elongated geometry of the nanowire, which leads to considerable suppression of the absorption of light polarised perpendicularly to the nanowire axis. The nanowires analyzed in this thesis are relatively thick, reducing the severity of this effect. However, matching the polarization direction with the nanowire orientation is still important.

After the excitation beam passed through the polarizer and the gray-filter, it was guided through a beam-splitter in order to make it possible to guide the signal from the sample towards the spectroscope later on. The beam-splitter converts the linearly polarized laser beam to elliptic polarization, but this does not eliminate the problem related to the dielectric mismatch effect mentioned above. If the elliptically polarized light has its minor axis point in the direction of the nanowires axis, absorption efficiency will still be suboptimal.

Further the excitation beam passed through an objective that allows focusing the laser beam onto a single nanowire and collects the signal emitted by the nanowire. The objective is infinity-corrected, meaning that the reflected beam in theory can travel arbitrarily long distance before being focused onto a detector.

The signal were then guided through the beam-splitter towards a new set of filters. The signal contains a strong contribution from the reflection of the excitation beam, so it was therefore important to reject the excitation beam using a high-pass filter before the spectroscope. For the samples where lasing was achieved, it was necessary to add another gray-filter before the spectroscope in order to prevent the high-sensitivity CCD detector from saturation.

In order to have sufficient excitation to the nanowire, an external laser was used in order to optically pump the nanowire. To make sure only one nanowire gets excited at a time

and that the selected nanowire gets sufficient excitation power, the excitation beam had to be concentrated down to a microscopic level. This was achieved with a long-working distance microscope objective as mentioned above. However, by doing so we also increase the heat generated at the sample, having a risk of damaging the sample. To prevent this from happening we used a pulsed laser device with approximately 120 fs pulse duration with a pulse frequency of 80 MHz. This corresponds to 12.5 ns between each successive pulses, letting the sample have enough time to relax completely between the pulses. It is worth mentioning that the power used in plots later on is an average value. The peak power of each pulse is on the scale of one hundred thousand times as much as the average power (!) due to the incredibly short duration of the pulses.

3.2 List of Equipment

- Excitation laser: Spectra Physics Tsunami Ti: sapphire fs/ps pulsed laser, tunable from 700-1000 nm, pumped by Spectra Physics Millennia eV 15 W continuous wave Nd:YVO4 (Yttrium Orthovanadate) operating at 1064 nm, which is frequency-doubled inside the cavity to yield an output beam at 532 nm.

- Objective: Mitutoyo NIR-optimised, infinity-corrected long-working distance (10 mm) microscope objective with magnification 50x and numerical aperture (NA) 0.65.

- Spectrograph: Horiba Jobin-Yvon iHR-550 Czerney-Turner type spectrograph, equipped with a 300 lines/mm grating blazed at $1\mu m$ wavelength which was used exclusively.

- Detection by an Andor Newton electron-multuplying (EM) CCD camera.

- Cryogenic setup: Janis ST-500 optical cryostat equipped with a 3D Attocube piezo positioning stage, coupled to a Cryo Industries closed cycle cryogenic cooler equipped with a He liquefier.

4 Analysis

A total of five nanowires were studied for each sample at low-temperature, with a total of three samples for each substrate (DBR and Si) - one for each thickness of silica spacer (0nm, 200nm and 400nm)(results for all NWs can be seen in the appendix). Two NWs on DBR and one NW on Si achieved lasing with no applied silica layer. For a 200nm thick silica layer, all the NWs on both the DBR and Si substrate achieved lasing. For a 400nm thick silica layer, only two NWs achieved lasing on the DBR substrate, while all studied NWs on the Si substrate lased.
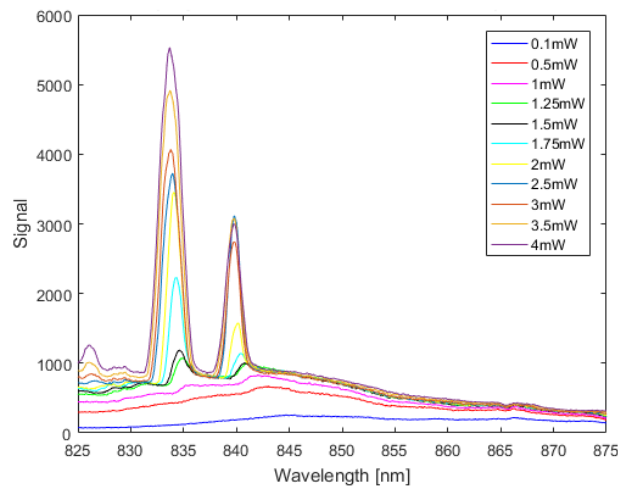
Figure 16: First nanowire lying on DBR substrate with no silica spacing between substrate and nanowire. Taken at $T = 20K$. Threshold excitation power: 1.75mW where FWHM: 1.377nm
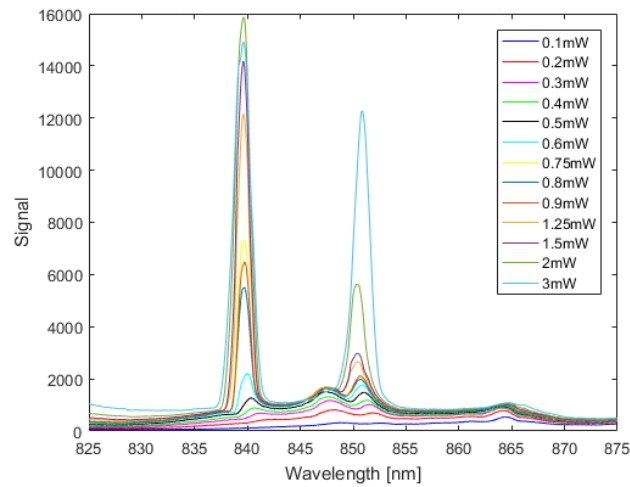
Figure 17: First nanowire lying on DBR substrate with 200nm silica spacing between substrate and nanowire. Taken at $T = 20K$. Threshold excitation power: 0.9mW where FWHM: 1.227nm
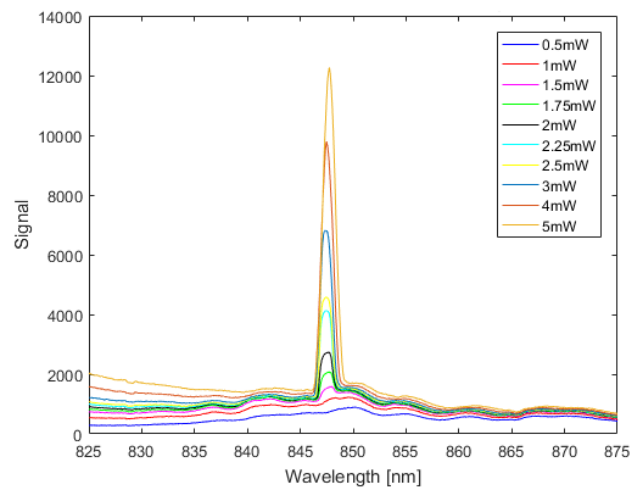
Figure 18: The third nanowire lying on DBR substrate with 400nm silica spacing between substrate and nanowire. Taken at $T = 20K$. Threshold excitation power: 2.25mW where FWHM: 1.300nm
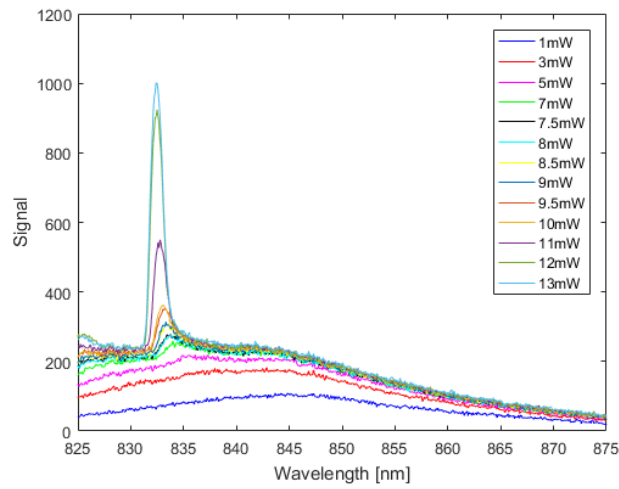
Figure 19: First nanowire lying on silicon substrate with no silica spacing between substrate and nanowire. Taken at $T = 50K$. Threshold excitation power: 9mW where FWHM: 1.445nm
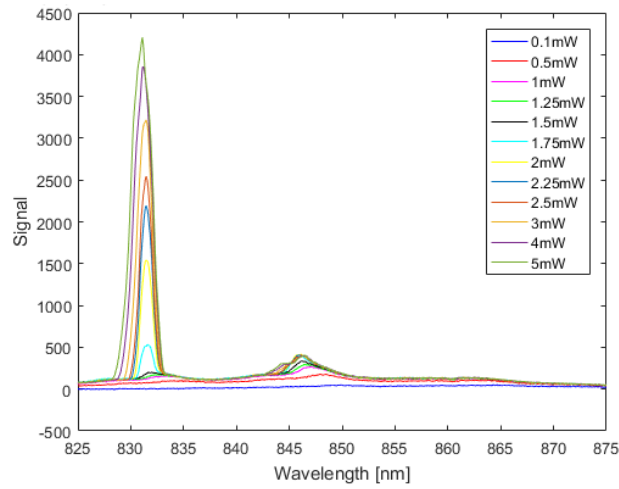
Figure 20: First nanowire lying on silicon substrate with 200nm silica spacing between substrate and nanowire. Taken at $T = 50K$. Threshold excitation power: 1.75mW where FWHM: 1.210nm
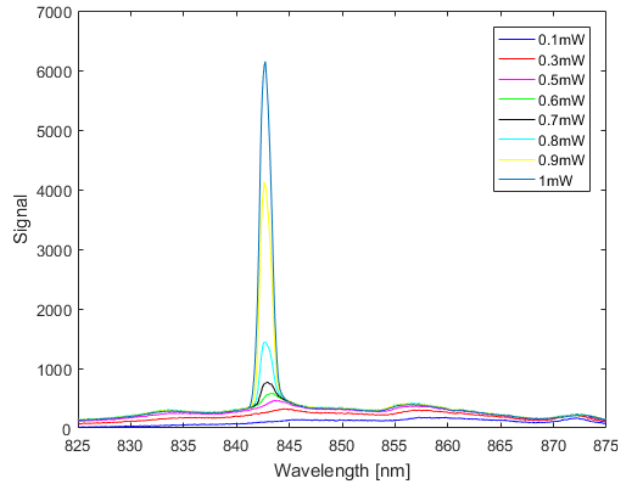
Figure 21: First nanowire lying on silicon substrate with 400nm silica spacing between substrate and nanowire. Taken at $T = 50K$. Threshold excitation power: 0.9mW where FWHM: 1.277nm

Between 0.1 mW and 20 mW excitation power was applied in order to study the NWs, varying for each NW based off what power level lasing was achieved. Close to the onset of lasing the interval between each power level was decreased in order to get a more detailed measurement of the lasing transition.

To prevent excitation damage to the NWs, low-temperatures of 20K and 50K were used while gathering data from the samples. The difference in temperature was unintentional, but due to technical issues with the liquid-helium equipment only 50K was achieved for the Si substrate. However, the temperature difference does not imply any dramatic change in the excitation conditions. For 20K, this gives a kT value of 1.72347 meV, while for 50K the kT value equals 4.30867 meV. In comparison, room temperature gives a kT value of 25.2488 meV.

4.1 Proof of Lasing
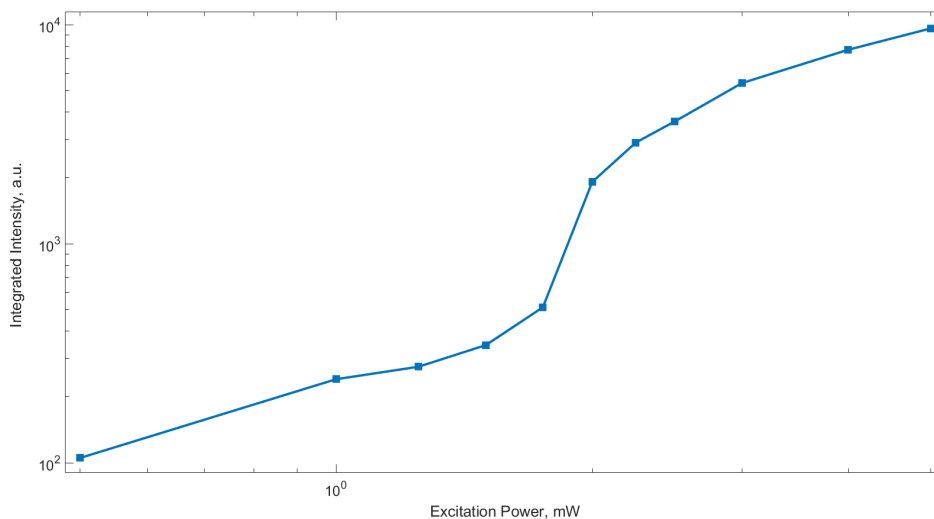
(a) The light-in-light-out curve is the integrated area beneath the lasing peaks plotted as a function of excitation power.
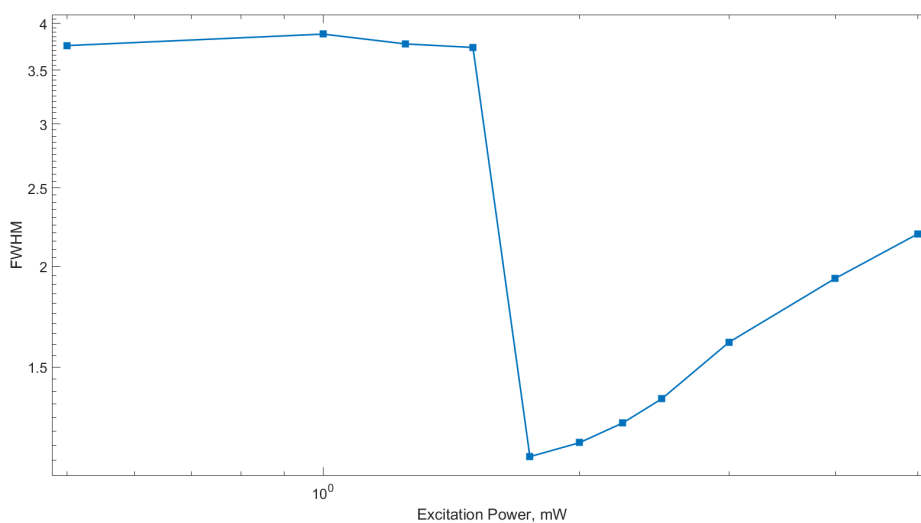
(b) Full width at half-maximum plotted as a function of excitation power.

Figure 22: Light-in-light-out curve and FWHM of lasing peaks for the first NW on the Si substrate. Both graphs are plotted with log-log axis.

To identify lasing of the NWs, two main characteristics are validated in order to confirm lasing. The representative NW in fig. 22 exhibits suspected single-mode lasing. First,

looking at figure 22a the integrated signal for each lasing peak are plotted as a function of the excitation power. The left-hand side of the curve represent the linear increase of spontaneous emission form the NW. The steeper slope region of the curve comes from amplified spontaneous emission. The linear right-hand side of the curve represent lasing, and the characteristic S-shape of the light-in-light-out curve is one of the signature features commonly used to recognize lasing.

Second, the figure 22b represent the full width at half-maximum values as a function of the excitation power. The sudden drop in FWHM values signifies the step-wise lineshape narrowing of the PL emission, which is another signature feature of lasing and its presence is another important criterion used commonly to recognize lasing. The excitation power at this point is defined as the effect threshold of lasing for the NW.

4.2 Threshold Comparison
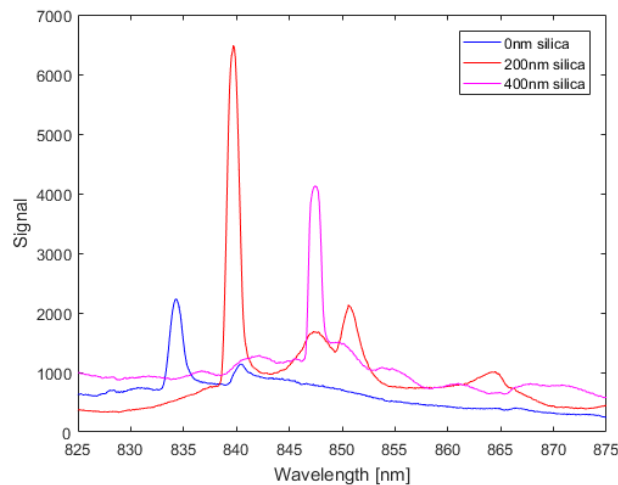
Figure 23: Comparison between the threshold curves for 0nm, 200nm and 400nm silica layers at DBR substrate.

Comparing signals at laser threshold can give important information about the influence of the substrate. In figure 23 the threshold curves at 0 nm, 200 nm and 400 nm silica layer for DBR are compared. The 0 nm silica sample yields lowest signal, possibly due to

coupling between the NW and the DBR. Since the DBR's refractive index are sufficiently large, light may leak into the substrate in the form of evanescent waves. It is therefore necessary to add a spacing between the substrate and the NW. With 400 nm of silica, the separation is probably too big, and leakage light from the NW does not reach the DBR in order to get reflected backwards. The 200 nm silica layer is as indicated by the fact that this substrate corresponds to the lowest threshold and the narrowest linewidth (FWHM).
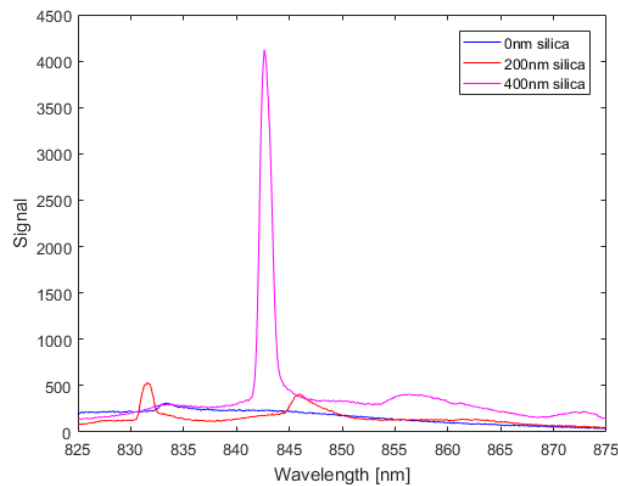
Figure 24: Comparison between the threshold curves for 0nm, 200nm and 400nm silica layers at silicon substrate.

In figure 24 the PL spectra just above threshold at 0 nm, 200 nm and 400 nm silica layer for silicon are compared. As Si is a light absorbing material for the lasing wavelength, so adding spacing between substrate and NW decreases the threshold.The lowest threshold is observed for 400 nm spacer thickness, indicating once more that coupling of the NW optical field to the substrate occurs for spacer thicknesses 0-200 nm.
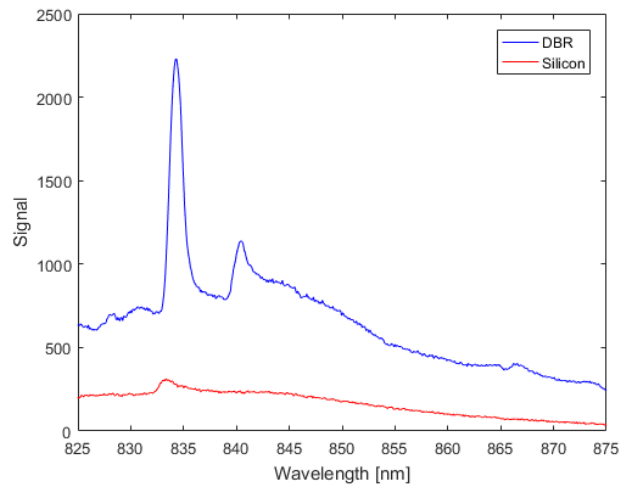
Figure 25: Comparison between the threshold for DBR and silicon substrate for no silica layer.
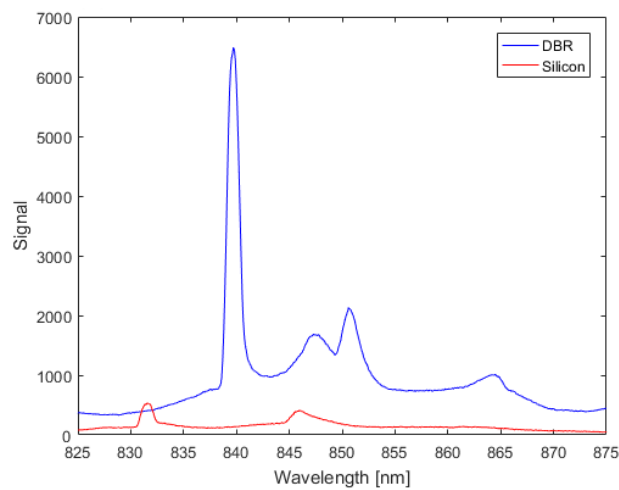
Figure 26: Comparison between the threshold for DBR and silicon substrate for 200nm silica layer.
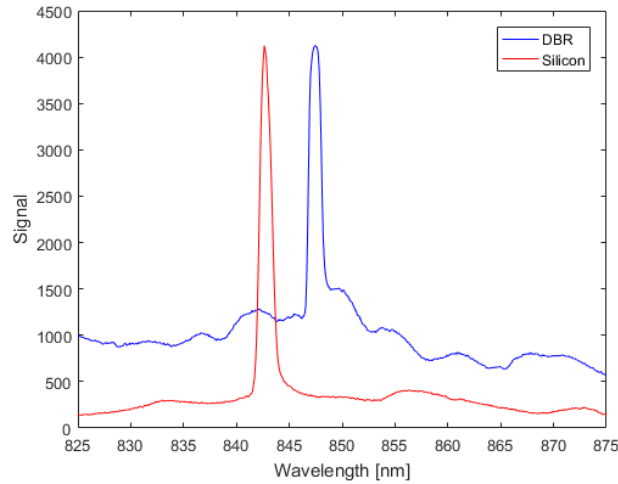
Figure 27: Comparison between the threshold for DBR and silicon substrate for 400nm silica layer.

Figures 25-27 compares PL spectra just above threshold for DBR and silicon for each thickness of the silica spacer. For NWs directly on the substrate (i.e. no spacer), the DBR improves dramatically the lasing performance by lowering the threshold. For 200 nm spacer, which corresponds to the lowest threshold observed for NWs on the DBR substrate, the lasing performance on DBR is still superior to that on Si. This indicates that while in the former case leakage light reaching the substrate is reflected and may re-enter the NW optical cavity, in the latter case it is absorbed, resulting in higher losses. For 400 nm spacer, the influence of the substrate on the lasing properties is negligible, and the only difference is the higher spontaneous emission plateau for the DBR sample. This is because the DBR substrate enhances the collection efficiency of the spontaneous emission, resulting in higher background signal in addition to the lasing peak.

It is worth mentioning that the DBR used is optimized for 950nm wavelength, which means that the present lasing wavelengths are at the edge, just outside of its high reflectivity band. Still, for most angles, and critically for large angles of incidence, reflectivity above 50% is expected.

Thickness of silica layer	DBR	Silicon
0nm	1.75mW	9mW
200nm	0.9mW	1.75mW
400nm	2.25mW	0.9mW

Table 1: Comparison of excitation power at threshold.

Thickness of silica layer	DBR	Silicon
0nm	1.377nm	1.445nm
200nm	1.227nm	1.210nm
400nm	1.300nm	1.277nm

Table 2: Comparison of FWHM at threshold.

Table 1 and 2 compares numeric values of excitation power and FWHM at threshold for the different substrates.

5 Conclusion

To conclude, for DBR substrate without a silica spacer the nanowire modes couple into the evanescent modes in the DBR, which is not desirable. If the silica spacer becomes too thick, the leakage light from the NW will not be able to reach the DBR, resulting in an increased threshold. Hence the lowest threshold and narrowest lineshape is found for NWs on DBR with a 200 nm silica spacer.

For the pure silicon substrate, the losses due to substrate absorption were too high, resulting in a very high threshold. As the spacer thickness is increased, threshold values decrease, indicating that the nanowire-substrate interaction is dramatically reduced for 400 nm silica threshold.

The best performance is achieved for 200 nm silica spacer on DBR. Future improvements are: use DBR optimized for the lasing wavelength, and grow NWs on DBR in order to achieve NW array lasing with a near-perfect bottom cavity mirror.

References

[1] Ren, Dingding and Ahtapodov, Lyubomir and Nilsen, Julie S. and Yang, Jianfeng and Gustafsson, Anders and Huh, Junghwan and Conibeer, Gavin J. and van Helvoort, Antonius T.J. and Fimland, Bjørn-Ove and Weman, Helge. *Single-Mode Near-Infrared Lasing in a GaAsSb-Based Nanowire Superlattice at Room Temperature* 2018.

[2] John D. Joannopoulos, Steven G. Johnson, Joshua N. Winn, and Robert D. Meade. *Photonic Crystals, Molding the Flow of Light, 2nd edition* November 13, 2007, page 44 - 63.

[3] John D. Joannopoulos, Steven G. Johnson, Joshua N. Winn, and Robert D. Meade. *Photonic Crystals, Molding the Flow of Light, 2nd edition* November 13, 2007, page 47.

[4] Lyubomir Ahtapodov. *Optical Properties of III-V Semiconductor Nanowire Structures* April, 2017, page 34.

[5] B. E. A Saleh and M. C. Teich. *Fundamentals of Photonics* 2nd edition, 2007, page 271.

[6] B. E. A Saleh and M. C. Teich. *Fundamentals of Photonics* 2nd edition, 2007, page 64.

[7] C. Kittel, "Introduction to Solid State Physics", 7th ed., Wiley, 1996

[8] M. Fox, "Optical Properties of Solids", Oxford University Press, 2001

[9] L. Ahtapodov, "Optical Properties of III-V Semiconductor Nanowire Structures", Doctoral Thesis at NTNU, 2017:241

[10] P.N. Prasad, "Nanophotonics", Wiley, 2004

[11] C.L. Tang, "Fundamentals of Quantum Mechanics for Solid State Electronics and Optics", Cambridge University Press, 2005

Appendices

A   Early Tested NWs
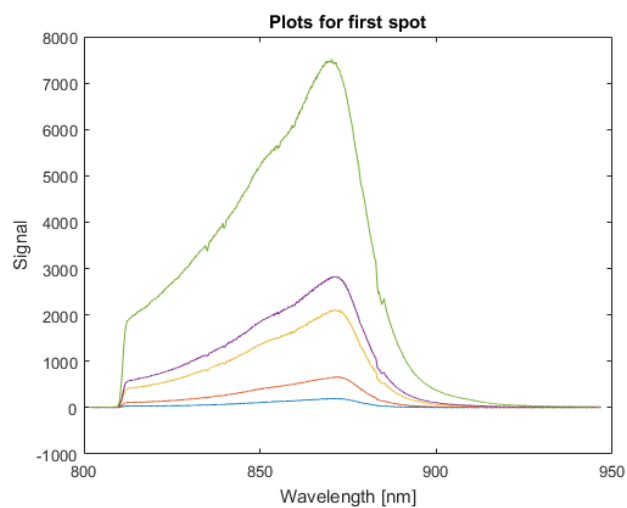
Figure 28: 2018-10-25: No lasing. Spontaneous emission from GaAsSb.
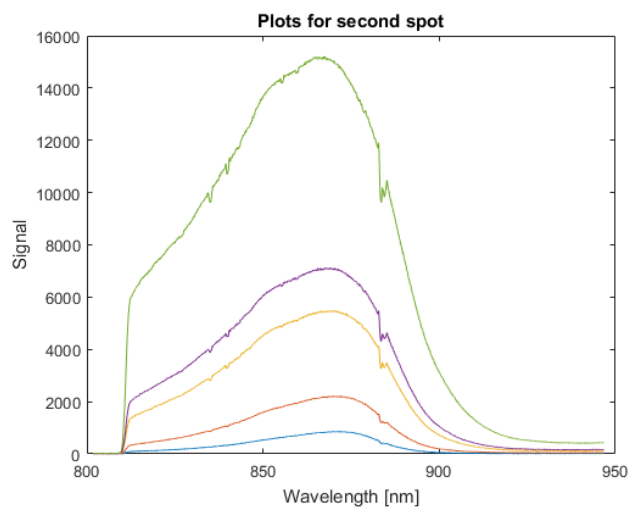
Figure 29: 2018-10-25: No lasing. Spontaneous emission from GaAsSb.
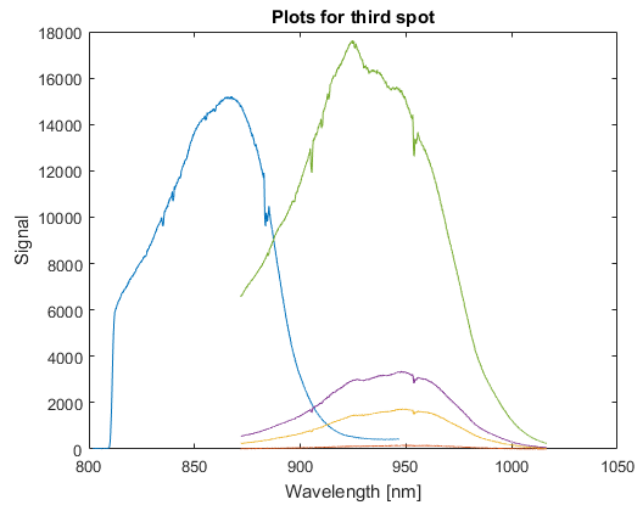
Figure 30: 2018-10-25: No lasing. Spontaneous emission from GaAsSb, shifting towards substrate excitation.
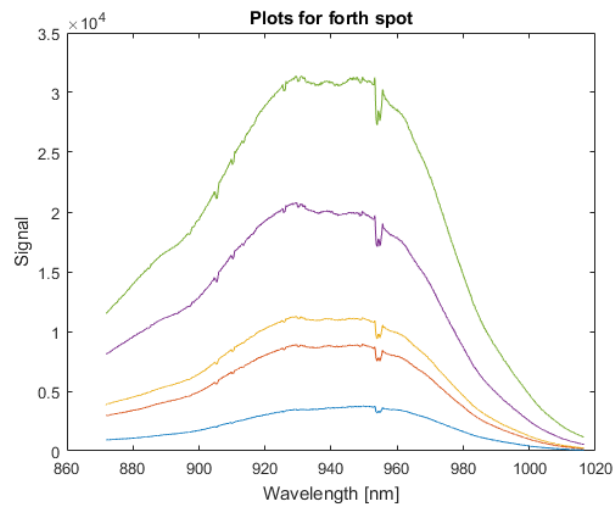
Figure 31: 2018-10-25: No lasing. Spontaneous emission from GaAsSb.
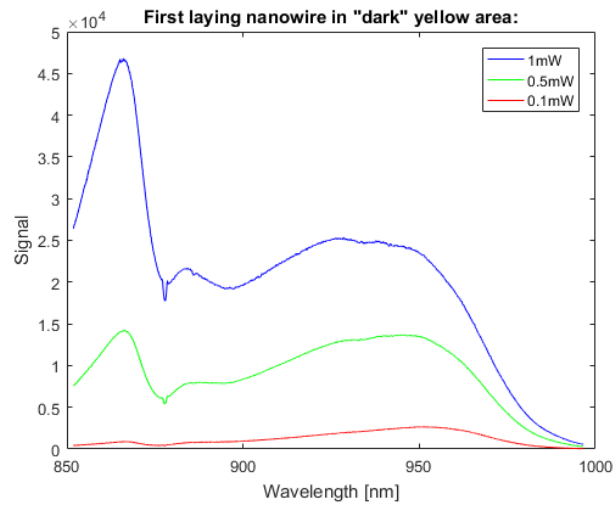
Figure 32: 2018-10-31: No lasing. Spontaneous emission from GaAsSb.
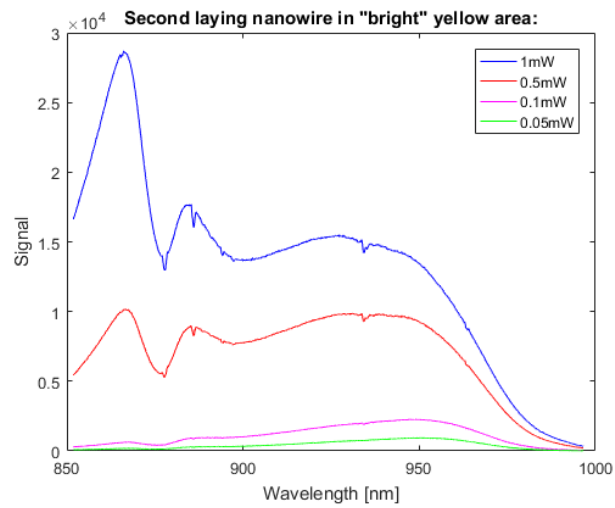
Figure 33: 2018-10-31: No lasing. Spontaneous emission from GaAsSb.

B   Possibly Lasing
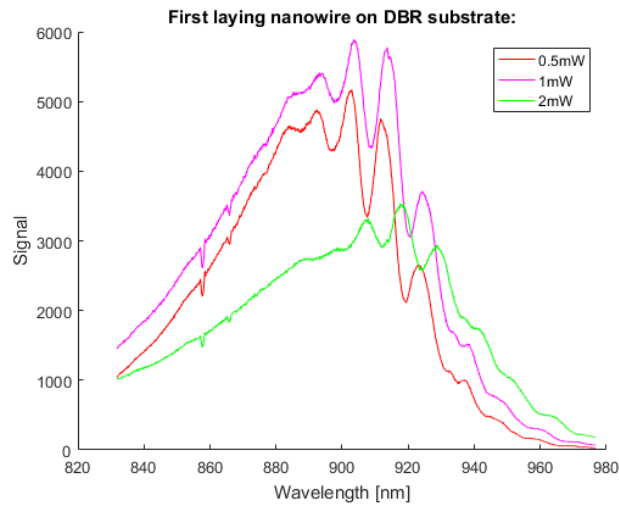
Figure 34: 2018-11-05: Nanowires lying on DBR. Fringes makes NW look promising.
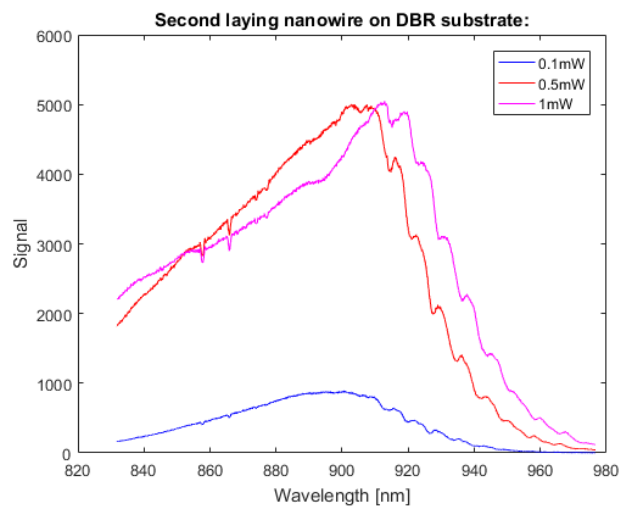
Figure 35: 2018-11-05: Nanowires lying on DBR. Fringes makes NW look promising.
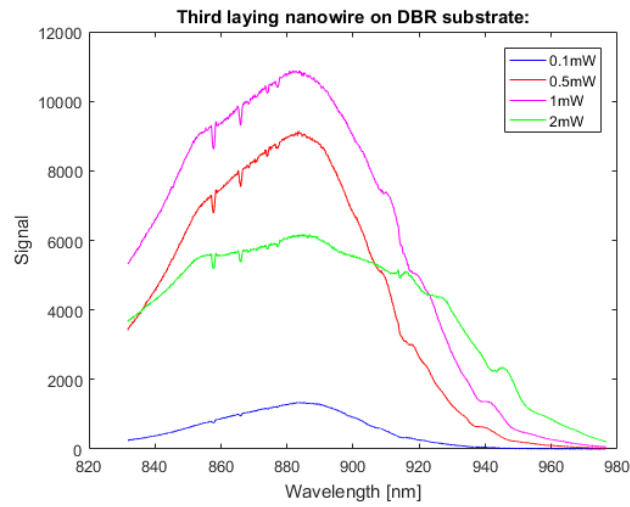
Figure 36: 2018-11-05: Nanowires lying on DBR. Fringes makes NW look promising.
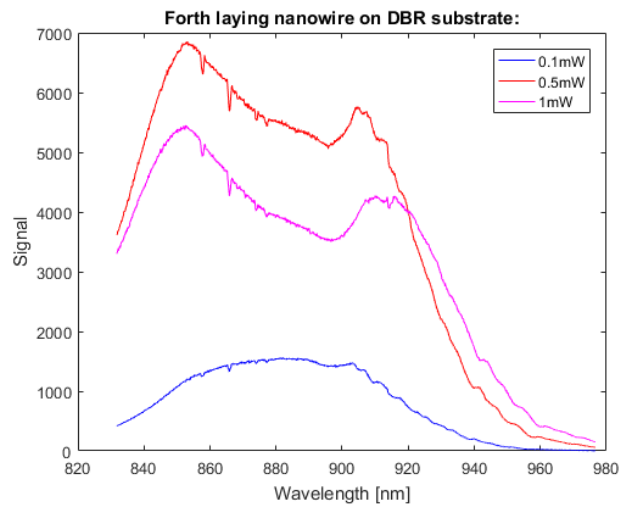
Figure 37: 2018-11-05: Nanowires lying on DBR. Normal excitation.
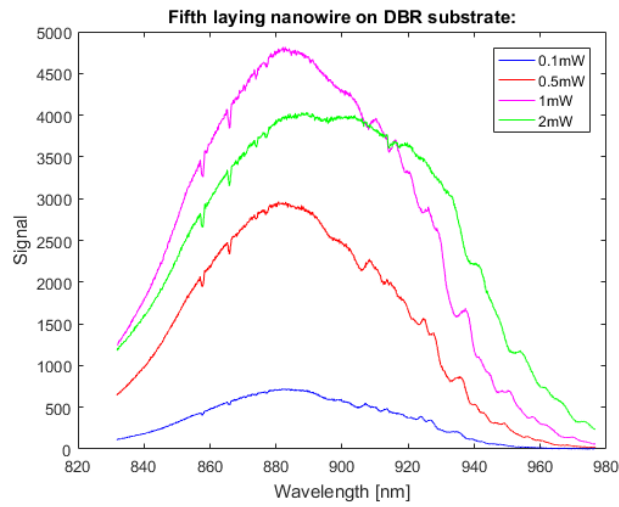
Figure 38: 2018-11-05: Nanowires lying on DBR. Fringes makes NW look promising.
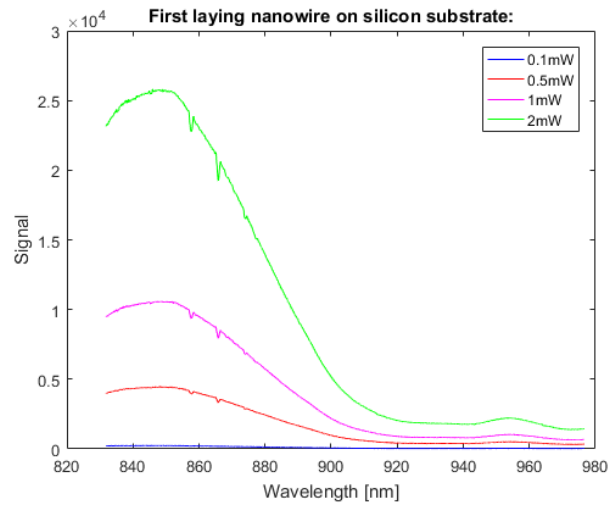
Figure 39: 2018-11-05: Only excitation of substrate.
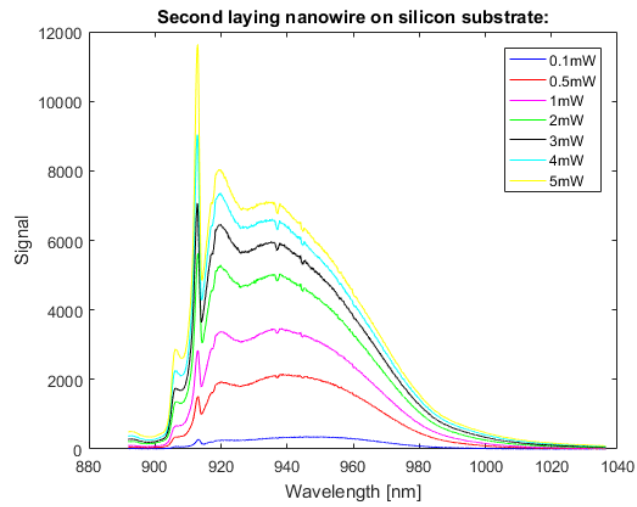
Figure 40: 2018-11-05: Possible lasing.
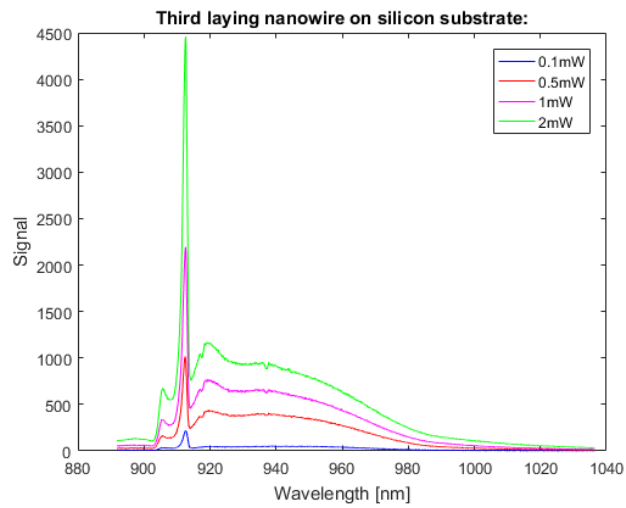
Figure 41: 2018-11-05: Possible lasing.
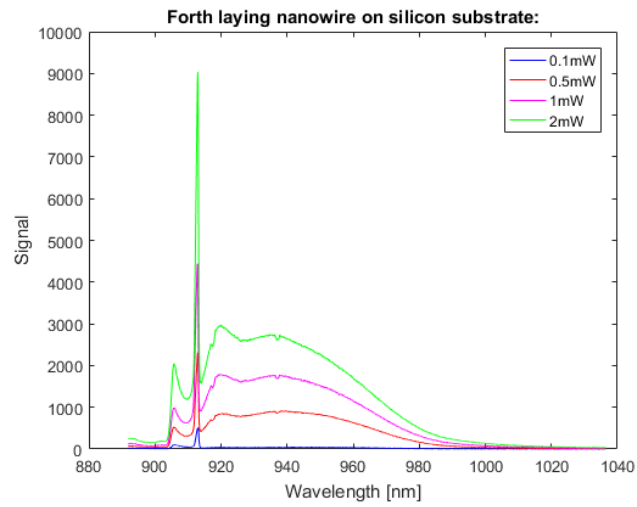
Figure 42: 2018-11-05: Possible lasing.

C Low-temperature of 20K
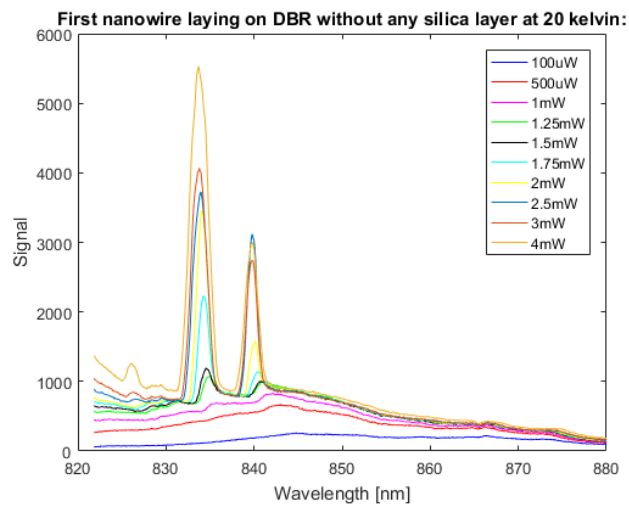
Figure 43: 2019-03-28: Lasing with 2 modes.
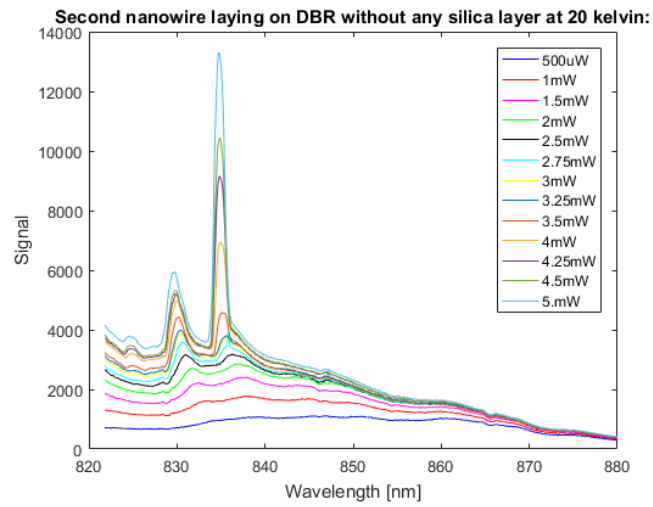
Figure 44: 2019-03-28: Lasing with 2 modes
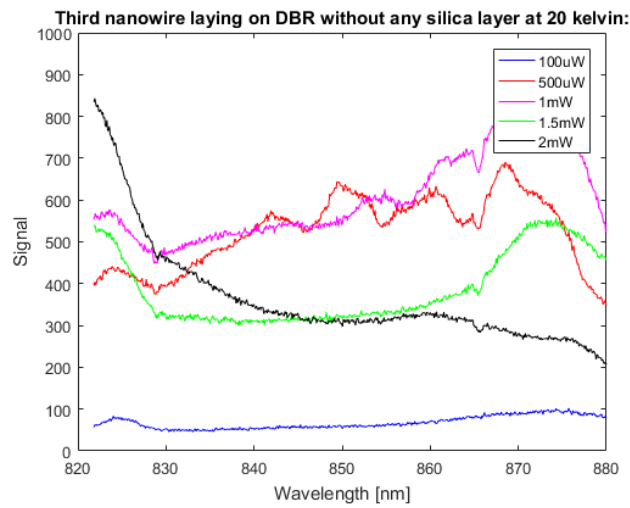
Figure 45: 2019-03-28: No excitation.
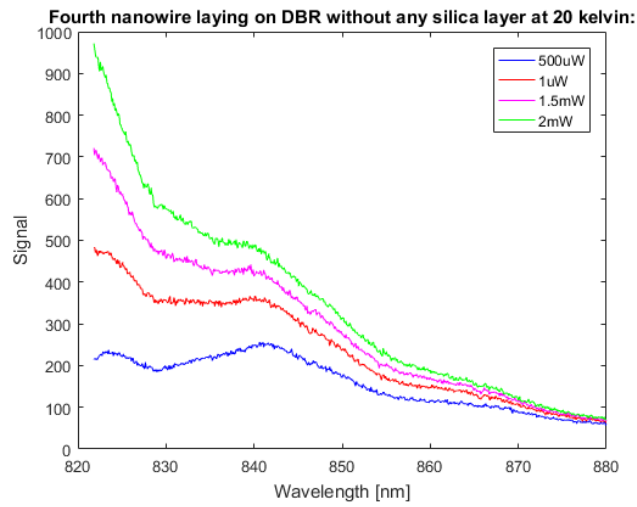
Figure 46: 2019-03-28: No excitation.
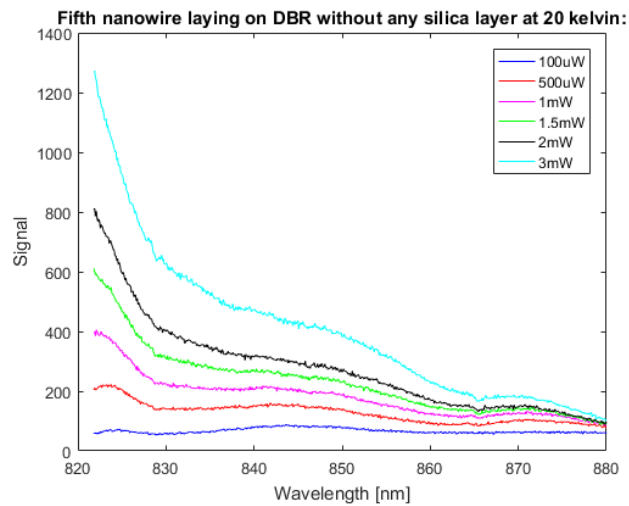
Figure 47: 2019-03-28: No excitation.
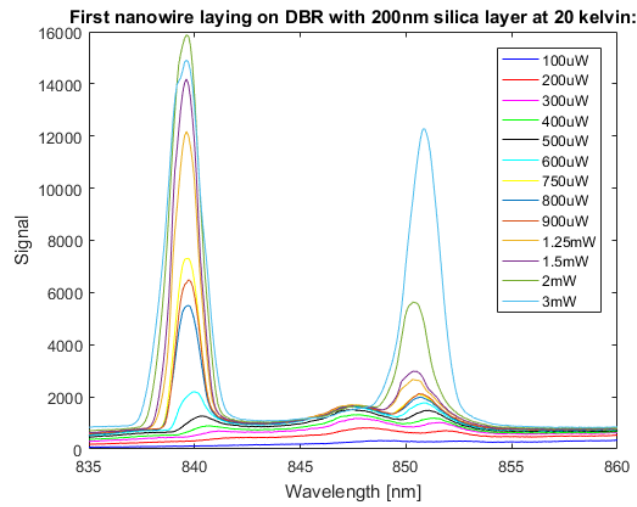
Figure 48: 2019-03-28: Very promising lasing with more than one mode.
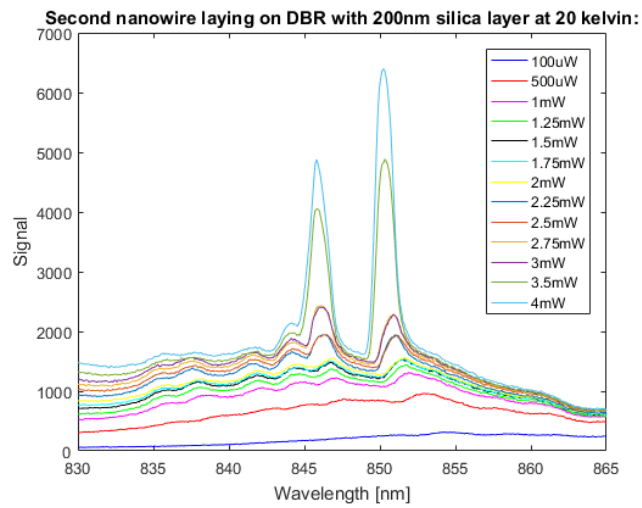
Figure 49: 2019-03-28: Very promising lasing with more than one mode.
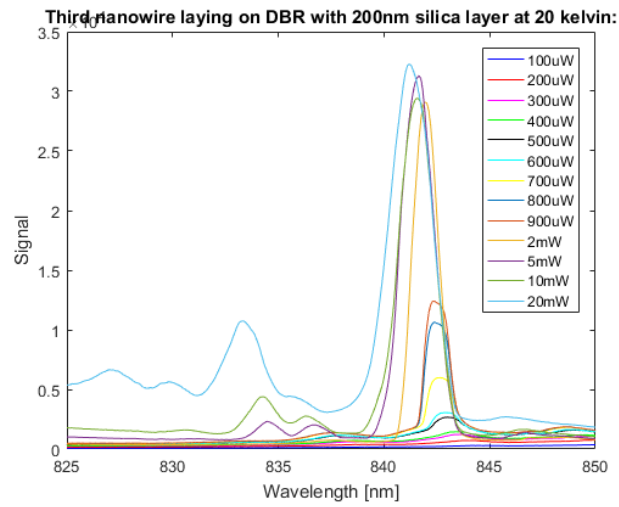
Figure 50: 2019-03-28: Very promising lasing with more than one mode.
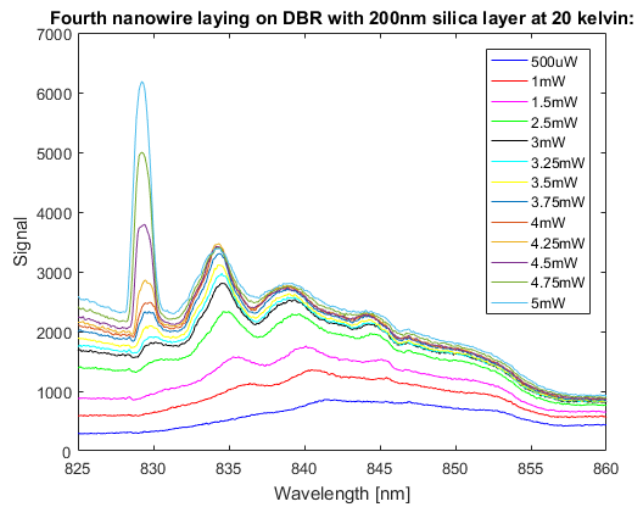
Figure 51: 2019-03-28: Very promising lasing with more than one mode.
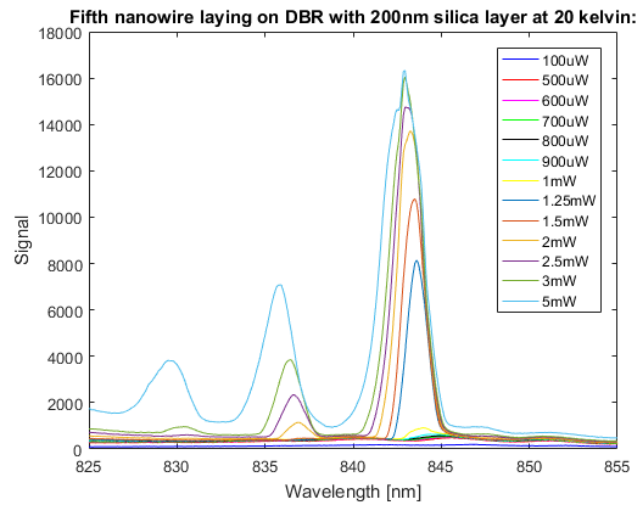
Figure 52: 2019-03-28: Very promising lasing with more than one mode.
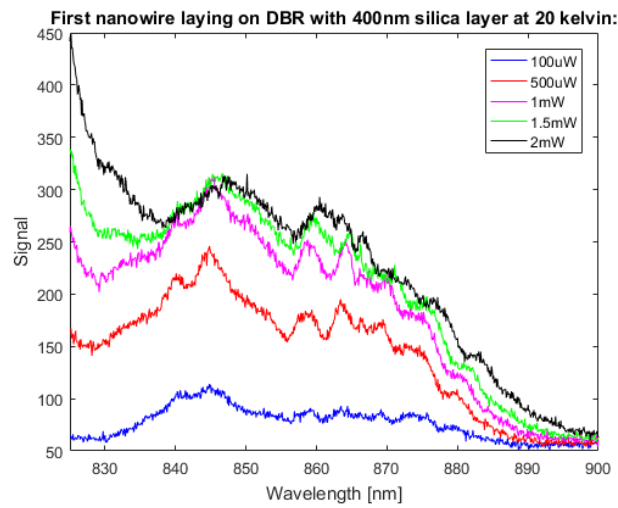
Figure 53: 2019-03-28: No excitation.
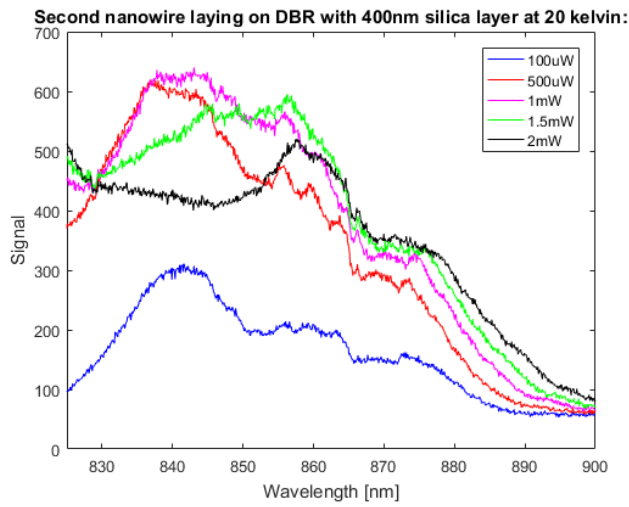
Figure 54: 2019-03-28: No excitation.
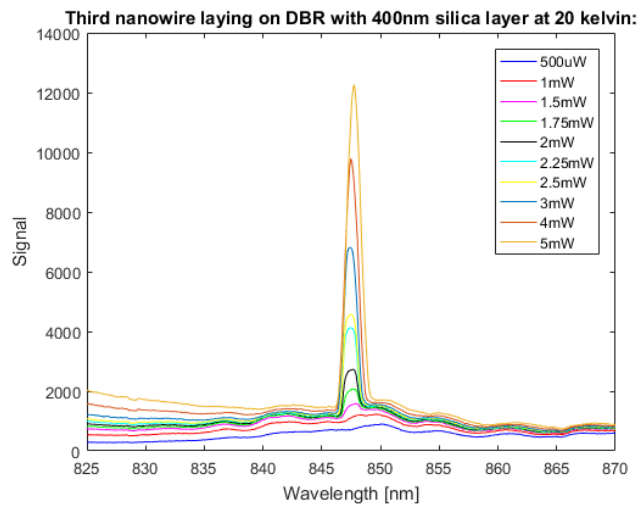
Figure 55: 2019-03-28: Very good lasing with one mode.
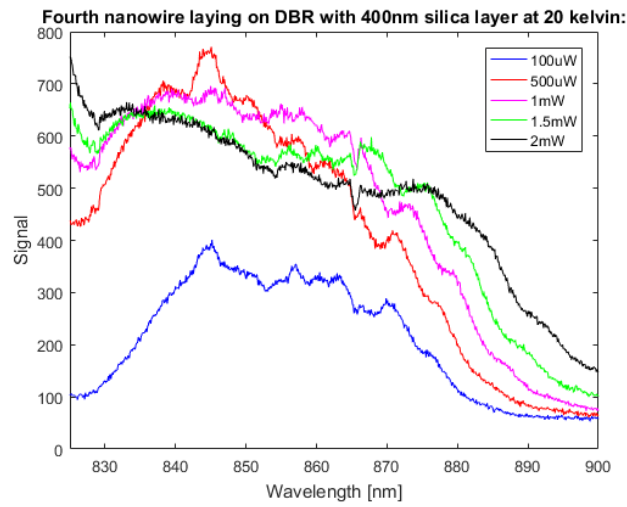
Figure 56: 2019-03-28: No excitation.
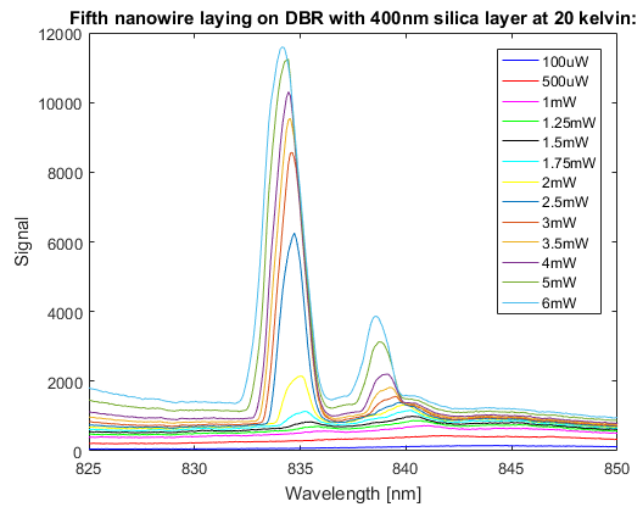
Figure 57: 2019-03-28: Very good lasing with 2 modes.

D Low-temperature of 50K
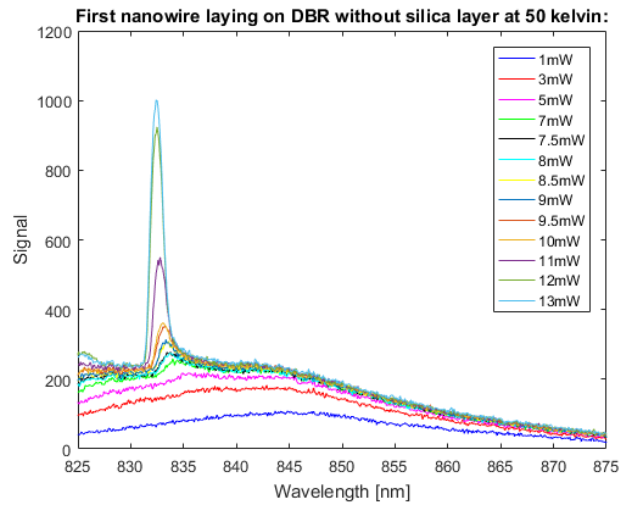
Figure 58: 2019-04-01: Lasing with one mode.
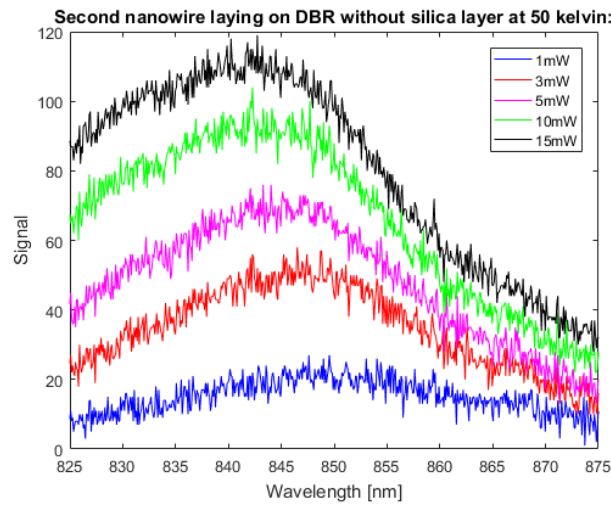
Figure 59: 2019-04-01: No excitation.
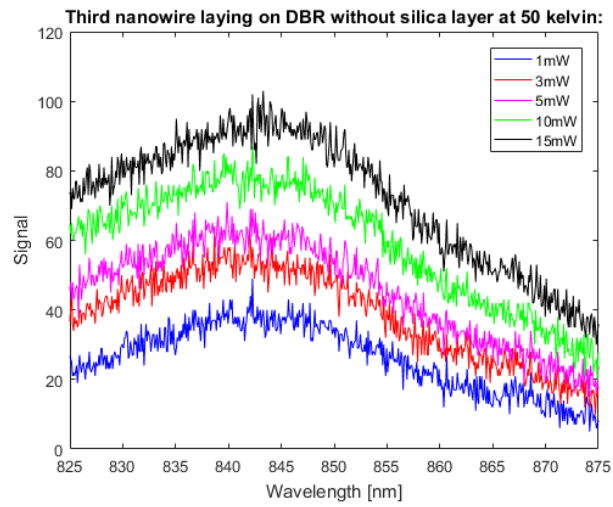
Figure 60: 2019-04-01: No excitation.
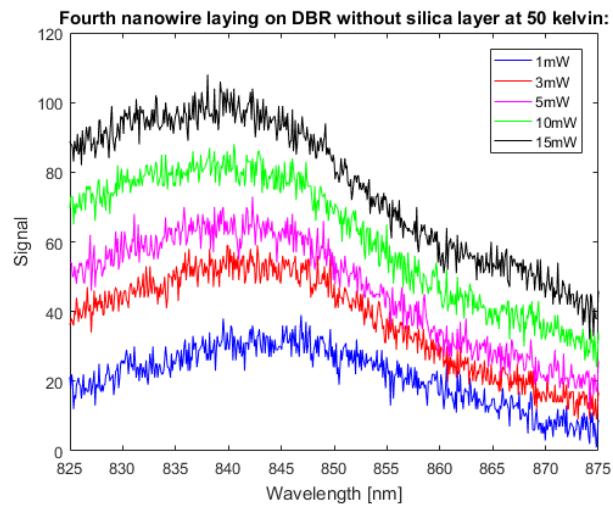
Figure 61: 2019-04-01: No excitation.
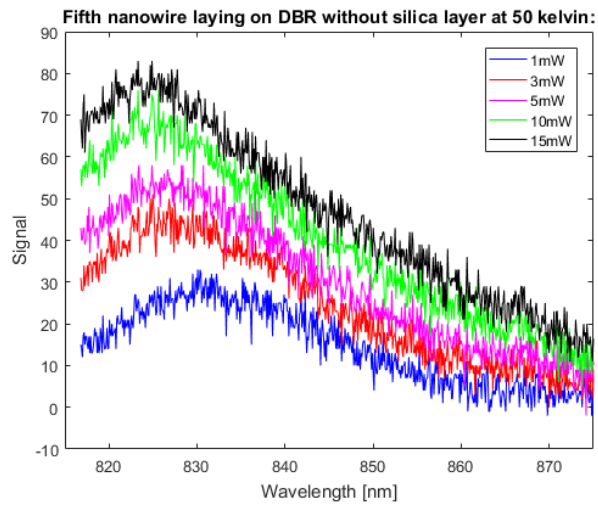
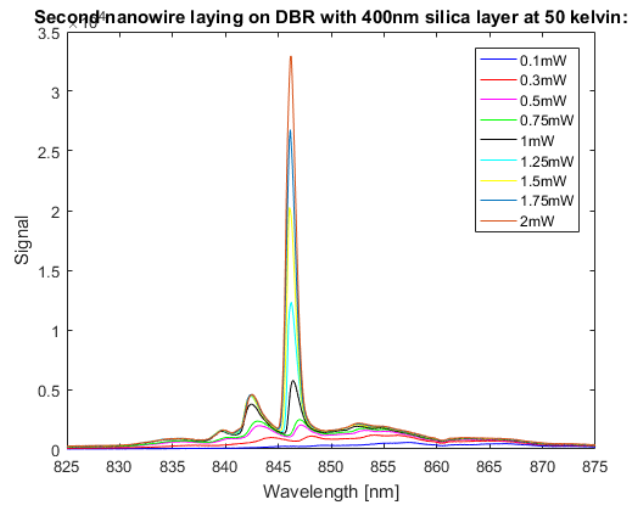**Figure 62:** 2019-04-01: No excitation.
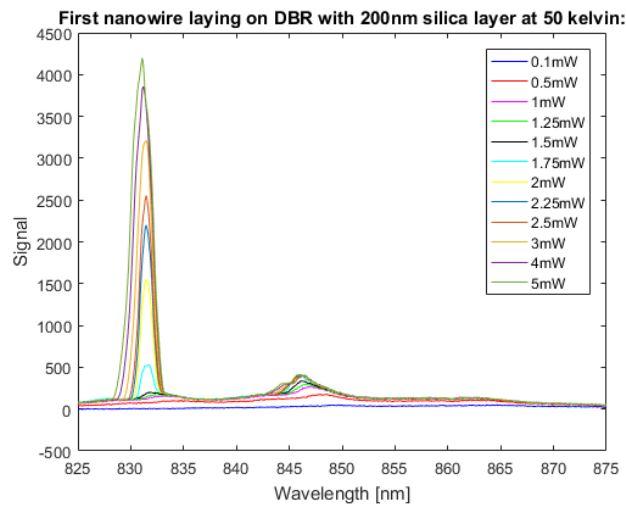
Figure 63: 2019-04-01: Very good lasing.
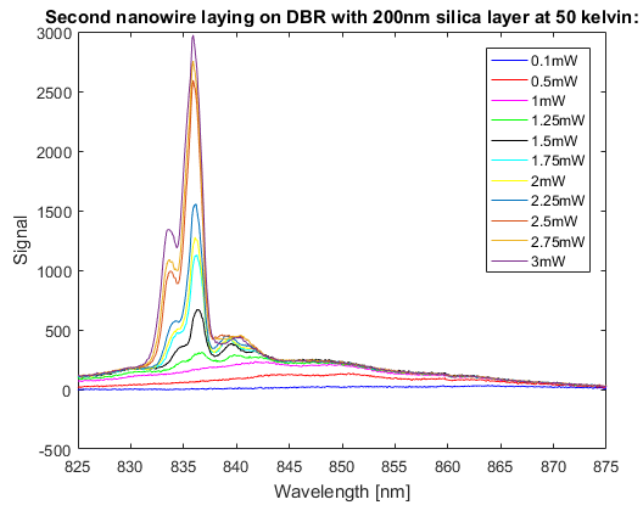
Figure 64: 2019-04-01: Very good lasing.
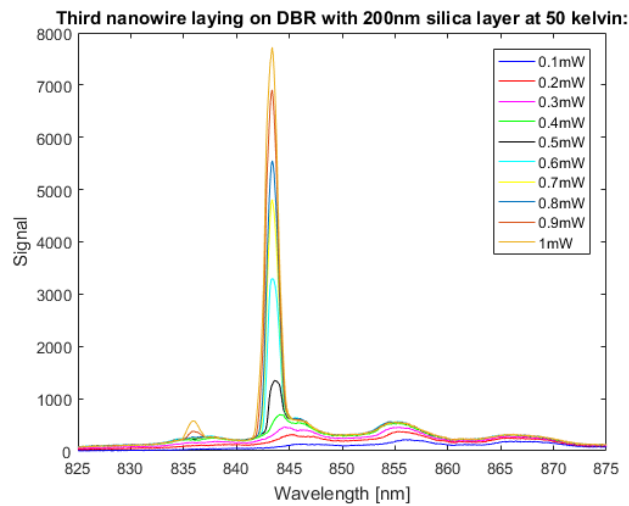
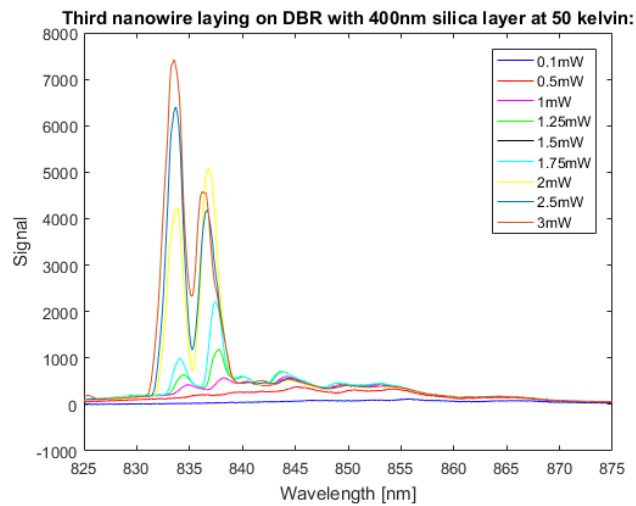

Figure 65: 2019-04-01: Very good lasing.
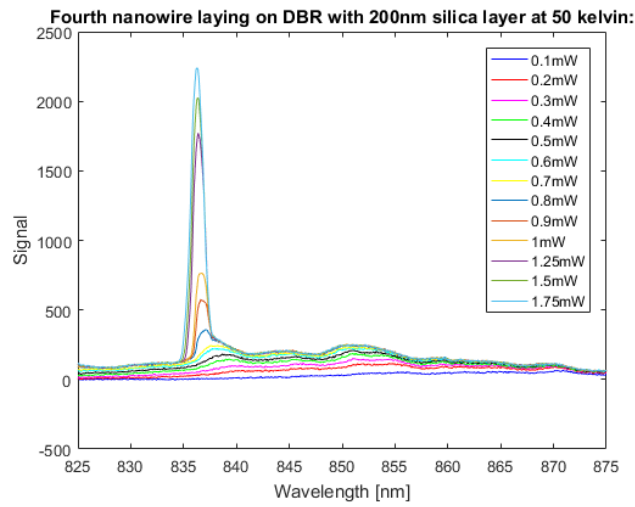
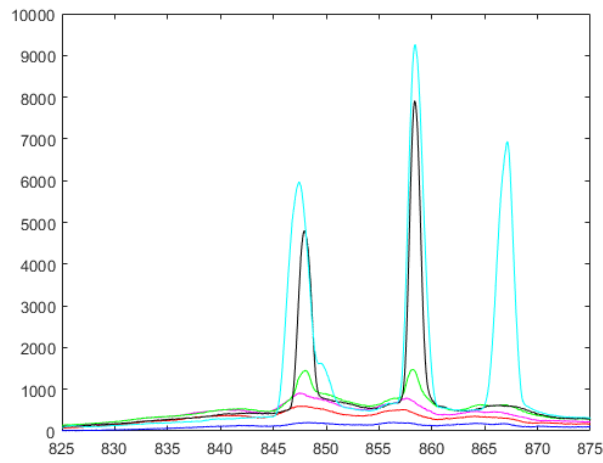**Figure 66:** 2019-04-01: Very good lasing.
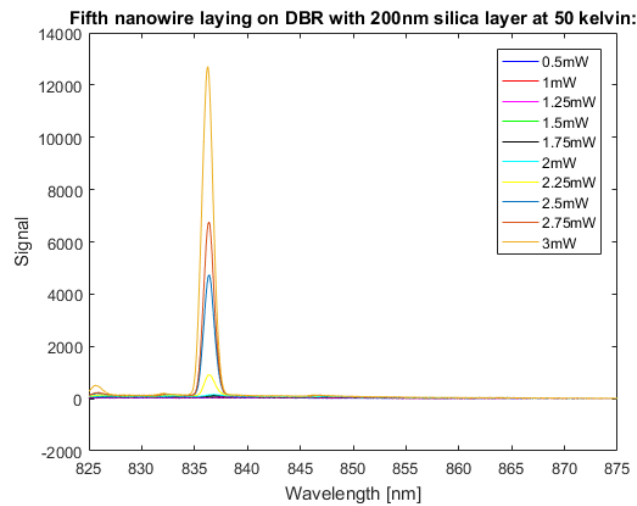
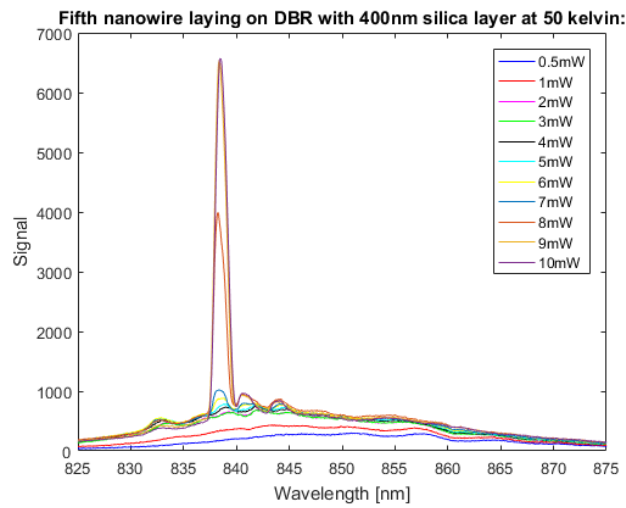**Figure 67:** 2019-04-01: Very good lasing.

Figure 68: 2019-04-01: Very good lasing.

Figure 69: 2019-04-01: Very good lasing.

Figure 70: 2019-04-01: Very good lasing.

Figure 71: 2019-04-01: Very good lasing.